AD-A049 958 SYSTEMS SCIENCE AND SOFTWARE LA JOLLA CALIF F/G 17/10
SEISMIC STUDIES OF SURFACE AND BODY WAVES FOR IMPROVED YIELD DE--ETC(U)
OCT 77 T C BACHE, W L RODI F08606-76-C-0041
UNCLASSIFIED SSS-R-78-3448 NL

| OF |
AD
A049958

END
DATE
FILMED
3-78
DDC

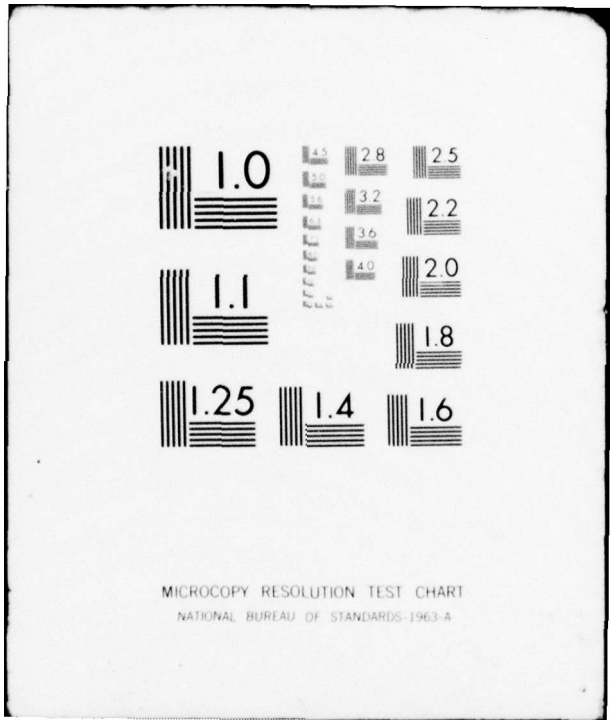
1.0
1.1
1.25
1.4
1.6
2.8
3.2
3.6
4.0
2.5
2.2
2.0
1.8
MICROCOPY RESOLUTION TEST CHART
NATIONAL BUREAU OF STANDARDS-1963-A

12

SYSTEMS, SCIENCE AND SOFTWARE

SSS-R-78-3448

SEISMIC STUDIES OF SURFACE AND BODY WAVES FOR IMPROVED YIELD DETERMINATION

T. C. BACHE
W. L. RODI

QUARTERLY TECHNICAL REPORT
FOR PERIOD JULY 1 - SEPTEMBER 30, 1977

SPONSORED BY
ADVANCED RESEARCH PROJECTS AGENCY
ARPA ORDER No. 2551

This research was supported by the Advanced Research Projects Agency of the Department of Defense and was monitored by AFTAC/VSC, Patrick Air Force Base, Flordia, 32925, under Contract No. F08606-76-C-0041.

OCTOBER 1977

P. O. BOX 1620, LA JOLLA, CALIFORNIA 92038, TELEPHONE (714) 453-0060

AFTAC Project Authorization No. VELA/T/7712/B/ETR

Program Code No. 6H189

Effective Date of Contract: October 1, 1976

Contract Expiration Date: September 30, 1978

Amount of Contract: $435,087

Contract No. F08606-76-C-0041

Principal Investigator and Phone No.
Dr. Thomas C. Bache, (714) 453-0060, Ext. 337

Project Scientist and Phone No.
Dr. Ralph W. Alewine, III, (202) 325-7581

UNCLASSIFIED

SECURITY CLASSIFICATION OF THIS PAGE (When Data Entered)

REPORT DOCUMENTATION PAGE

READ INSTRUCTIONS BEFORE COMPLETING FORM

1. REPORT NUMBER	2. GOVT ACCESSION NO.
3. RECIPIENT'S CATALOG NUMBER	
4. TITLE (and Subtitle)	5. TYPE OF REPORT & PERIOD COVERED
SEISMIC STUDIES OF SURFACE AND BODY WAVES FOR IMPROVED YIELD DETERMINATION	Quarterly Report 1 Jul - 30 Sep 77, 7/1/77 - 9/30/77
	6. PERFORMING ORG. REPORT NUMBER SSS-R-78-3448
7. AUTHOR(s)	8. CONTRACT OR GRANT NUMBER(s)
T. C. Bache W. L. Rodi	F08606-76-C-0041
9. PERFORMING ORGANIZATION NAME AND ADDRESS	10. PROGRAM ELEMENT, PROJECT, TASK AREA & WORK UNIT NUMBERS
Systems, Science and Software P. O. Box 1620 La Jolla, California 92038	Program Code 6H189 Project Authorization No. VELA/T/7712/B/ETR
11. CONTROLLING OFFICE NAME AND ADDRESS	12. REPORT DATE
VELA Seismological Center 312 Montgomery Street Alexandria, Virginia 22314	October 1977
	13. NUMBER OF PAGES 79 88 p.
14. MONITORING AGENCY NAME & ADDRESS (if different from Controlling Office)	15. SECURITY CLASS. (of this report) Unclassified
	15a. DECLASSIFICATION/DOWNGRADING SCHEDULE

16. DISTRIBUTION STATEMENT (of this Report)

Approved for public release, distribution unlimited.

17. DISTRIBUTION STATEMENT (of the abstract entered in Block 20, if different from Report)

DDC RECEIVED FEB 15 1978 F

18. SUPPLEMENTARY NOTES

19. KEY WORDS (Continue on reverse side if necessary and identify by block number)

Seismic surface waves
Seismic body waves
Geophysical inversion
Crustal structure
Theoretical seismogram generation
m_b versus yield
Cratering explosions
Small-scale explosion experiments

20. ABSTRACT (Continue on reverse side if necessary and identify by block number)

Work done during the period from 1 July to 30 September 1977 is summarized. The report also includes an Appendix in which are collected the abstracts of all reports submitted to the VELA Seismological Center since May 1975 (eight quarterly technical reports, two final contract reports and thirteen special topical reports).

DD FORM 1 JAN 73 1473 EDITION OF 1 NOV 65 IS OBSOLETE

UNCLASSIFIED

SECURITY CLASSIFICATION OF THIS PAGE (When Data Entered)

388 569

20. Abstract (continued)

The majority of the report is devoted to describing the results of two research projects not previously reported. One of these, "Determination of Crustal Structure from Surface Wave Dispersion Data," describes a recently developed method for obtaining crustal structure and gives results from application of this method to two paths in the southwestern United States: Nevada Test Site (NTS) to Albuquerque, New Mexico and NTS to Tucson, Arizona. Phase and group velocities are determined from NTS explosion recordings. These data are used in a formal generalized inversion procedure to determine crustal structures that are also consistent with other available data about the region; e.g., P_n velocities. Theoretical seismograms computed with the new crustal models show remarkable agreement with observations of NTS explosions at the two stations.

The second research study described is entitled "Small-Scale Laboratory Simulations of Explosion Produced Body Waves - Implications for the Teleseismic Signatures of Underground Nuclear Explosions." Small-scale laboratory experiments were carried out to measure the ground motions from spherical charges. There were two classes of experiments; one in which the ground motions were free-field and one in which they included a free surface effect. Of the latter, some were quite shallow and cratered. The most important feature of the experimental data is a large negative pulse that occurs at late-time in the experiments that include free-surface effects. Much of the study is directed toward determining the effect a pulse of this kind would have on the teleseismic body waves from nuclear explosions and m_b-log yield relations. If a late arriving negative pulse like that in the experimental data also occurs in underground nuclear explosions, the effect is to lower the slope of the m_b-log yield relation. This may explain why observed slopes are lower than predicted by theoretical models in which the free surface is represented elastically.

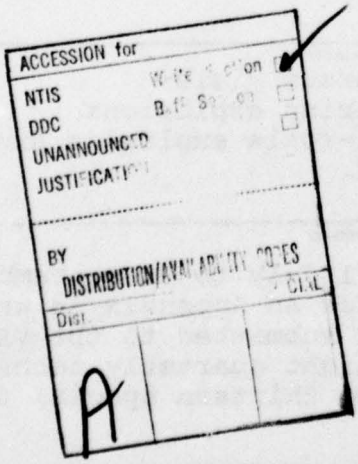

TABLE OF CONTENTS

TABLE OF CONTENTS (continued)

LIST OF ILLUSTRATIONS

LIST OF ILLUSTRATIONS (continued)

LIST OF TABLES

I. INTRODUCTION AND SUMMARY

1.1 BACKGROUND

The objective of our research program is to examine the parameters that affect the seismic signals from underground explosions. Attention is primarily directed to those features of the seismic waveforms that reliably indicate the explosion yield. Current research includes empirical studies of the available data, time signal analysis, experimental studies using small charges to simulate explosions and the development and application of theoretical and numerical methods. Emphasis is on the last of these. In particular, we are applying techniques for theoretically simulating the far-field signals from simple and complex seismic sources.

This report summarizes the work done during the fourth three-month period of our current contract. Closely related work was done on a previous contract which extended from May 1975 to October 1976. Since we are at the end of a year's work, it is a good time to summarize the work accomplished. For this purpose the abstracts of the reports submitted since May 1975 are collected in Appendix A.

1.2 MAJOR ACCOMPLISHMENTS DURING THIS QUARTER

One topical report was submitted during the last quarter: "Identification of Individual Events in a Multiple Explosion for Teleseismic Short Period Body Wave Recordings," by D. G. Lambert and T. C. Bache. This report gave the results of a study in which we attempted to detect and identify the individual events in a hypothetical multiple explosion. The teleseismic short period records were prepared at the VELA Seismological Center (VSC) and given to us in digital form. We analyzed these data

and identified several individual events. At this time we do not know the actual array configuration for comparison with our solution. The abstract of this topical report appears in Appendix A.

In Sections II and III of this quarterly report are the results of two research projects that have not previously been reported. Section II describes a recently developed method for determining crustal structure from surface wave dispersion data and gives results for application of this method to two paths in the southwestern United States. In Section III we present an analysis of some results from our small-scale laboratory simulations of explosion-produced body waves. In particular, we are concerned with the implications of these experiments for the signatures of underground nuclear explosions. In the remainder of this section we will summarize the important results from these two investigations.

1.3 SUMMARY OF SECTION II: "DETERMINATION OF CRUSTAL STRUCTURE FROM SURFACE WAVE DISPERSION DATA"

The objective of the work was to develop a reliable and convenient method for determining those features of the crust that control the amplitude and waveform of the Rayleigh waves propagated along particular paths. If such a method were available for studying explosion recordings, the source level, which depends on the yield, could be determined with increased confidence.

The method described in Section II is to use the information contained in the explosion-induced Rayleigh wave recordings themselves to deduce the characteristics of the path traversed by these Rayleigh waves. The phase and group velocity dispersion for each path is determined by a direct

analysis of the seismograms. These data are then used in a formal generalized inversion procedure to determine the crustal structure.

The method was tested for two paths; Nevada Test Site to Albuquerque, New Mexico (NTS-ALQ) and NTS to Tucson, Arizona (NTS-TUC). For each path a crustal structure was found that is consistent with other available data about the region. More important, theoretical seismograms computed with these earth models show remarkable agreement with the observations of NTS explosions at the two stations.

It seems reasonable to suppose that these methods can be successfully applied to any source region-receiver path of interest. The implications for determining the source amplitude, and hence yield, will be discussed in a forthcoming (classified) topical report.

1.4 SUMMARY OF SECTION III: "SMALL-SCALE LABORATORY SIMULATIONS OF EXPLOSION-PRODUCED BODY WAVES - IMPLICATIONS FOR THE TELESEISMIC SIGNATURES OF UNDERGROUND NUCLEAR EXPLOSIONS"

In previous quarterly reports we have described a series of small-scale laboratory experiments directed toward developing an improved understanding of the effect of depth of burial on the seismic signatures of underground nuclear explosions. There were two distinct classes of experiments. In the first class the recorded ground motion was essentially free-field; that is, uncontaminated by the effects of a free surface. In the second class the charges were detonated near a free surface. Of the latter, some of the charges were at shallow depths and cratered, while the others were contained.

The most striking feature of the experimental data is a large negative pulse that occurs at late times in the experiments in which the free-surface effects are present. In

Section III we study the effect a pulse of this kind might have on the teleseismic body wave signatures of nuclear explosions. Further, we estimate how it might affect m_b-log yield relationships.

If nuclear explosions have a large, late-arriving negative pulse like that seen in the experimental data, our analysis indicates that the effect would be to lower the slope of the m_b-log yield relation. This may provide an explanation of why the observed slopes are lower than those predicted by theoretical models in which the free surface is represented elastically.

II. DETERMINATION OF CRUSTAL STRUCTURE FROM SURFACE WAVE DISPERSION DATA

2.1 INTRODUCTION

Our objective in this work is to develop a reliable and convenient method for determining those features of the crust that control the amplitude and waveform of the Rayleigh waves propagated along particular paths. Of course, there is intrinsic interest in improved methods for inverting for earth structure from surface wave observations. Further, models that accurately account for amplitude attenuation are particularly valuable for problems that arise in monitoring underground nuclear explosions.

Using Rayleigh wave recordings of Nevada Test Site (NTS) explosions at the WWSSN Stations ALQ (Albuquerque, New Mexico) and TUC (Tucson, Arizona), we infer the crustal structure for the NTS-ALQ and NTS-TUC paths. The earth models for these paths are constructed by a formal inversion of phase and group velocity data which are determined from direct analysis of the seismograms.

These paths, or portions of them, have been studied by a number of previous investigators using body waves (e.g., Prodehl, 1970; Warren, 1969; Langston and Helmberger, 1974) or surface waves (e.g., Keller, et al., 1976; Alexander, 1964) and these previous solutions provide a useful check. However, our inversion is unique in a number of ways. First, both phase and group velocity data are used, providing a data set with considerably greater resolving power than group velocities alone. The formulation and solution of the inversion problem is done by a more efficient and flexible method then previously used. Further, an interesting verification of the models is provided by the fact that they give theoretical seismograms that show remarkable agreement with the observations.

Conventional surface wave theories (e.g., Harkrider, 1964) are unable to compute surface waves in a consistent way when events in close proximity have markedly different materials in the immediate vicinity of the source. Therefore, we begin by constructing, albeit in a somewhat ad hoc way, a theory in which two structures are used to model the source-receiver travel path. The amplitude excitation is computed in one structure - the source structure - and the dispersion is computed in the other - the path structure. A transmission coefficient accounts for passage of Rayleigh waves between the two.

Both phase and group velocities can be rather easily determined from explosion recordings because the phase and group delays at the source are nearly zero. The methods for determining group velocities (narrow band filtering) and phase velocities (unwrapping the phase spectrum) produce nearly independent estimates for the two velocities. Nevertheless, the velocities determined from the ALQ and TUC seismograms were quite constant from event to event and in excellent agreement with the differential relationship between phase and group velocity.

The models found by the inversion are rather simple (few sharp discontinuities are present) and are consistent with refraction data where it is available. The NTS-TUC path is characterized by a crustal thickness of 31 km while the average crustal thickness for NTS-ALQ is 42 km. The phase and group velocity data are all fit within 0.01 km/sec. The phase velocity data are especially important if theoretical seismograms are to match the observations. For example, a seismogram, the same seismogram inverted, and its Hilbert transform all have the same group velocity dispersion.

2.2 RAYLEIGH WAVES FROM PROXIMATE EVENTS IN DISSIMILAR SOURCE MATERIALS

A computationally convenient formulation of the theory for the surface waves generated by a point source in a plane-layered earth model was given by Harkrider (1964, 1970). The formulation of the theory is entirely in terms of linear elasticity, though the effect of anelastic attenuation can be included via an empirically determined Q operator. The source representation may be in terms of elementary point forces (Harkrider, 1964) or a general expansion of the outgoing elastic waves in terms of spherical harmonics (Harkrider and Archambeau, 1977). For spherically symmetric explosions a convenient source representation is the reduced displacement potential $\Psi(\tau)$ defined by

$$u(R,t) = \frac{\partial}{\partial R}\left(\frac{\Psi(\tau)}{R}\right), \qquad \tau = t - R/\alpha \quad , \tag{2.1}$$

where u is radial displacement, t is time, α is the P wave velocity and R is the distance from the explosion.

For direct application of the surface wave theory the entire source-receiver travel path is modeled as a single plane layered medium. The Fourier-transformed vertical component of the fundamental mode Rayleigh wave generated by a spherically symmetric explosion buried at depth h can then be written

$$\hat{w}(r,\omega) = - 4\Pi\mu_s \, \hat{\Psi}(\omega) \, \frac{K_s(h)\underset{\sim}{A}_R}{c} \, H_o^{(2)}\left(\frac{\omega r}{c}\right) , \tag{2.2}$$

where μ_s is the shear modulus of the source layer, r is epicentral distance, c is the phase velocity, $\dot{\Psi}$ is the time derivative of Ψ and a positive w displacement is upward. The amplitude response of the layered medium is represented by the real, positive quantities $\underset{\sim}{A}_R$, which is source-depth independent, and $K_s(h)$. Harkrider (1970) tabulates c, $\underset{\sim}{A}_R$ and K_s for several representative earth models. Finally, to account for anelastic attenuation and the sphericity of the earth, $\hat{w}(r,\omega)$ is multiplied by

$$e^{-\gamma r}\left(\frac{r}{a_e \sin \Delta}\right)^{1/2} , \qquad (2.3)$$

where γ is an empirically determined attenuation factor, Δ is range in degrees and a_e is the radius of the earth.

To use Equation (2.2) we need an average earth model for the source-receiver travel path of interest. While this approximation is satisfactory for studying dispersion, amplitudes cannot be computed in a consistent way when the material near the source is not the same as that at the source depth in the average path model. This problem is particularly important for nuclear explosion seismology where there is considerable interest in the relative amplitudes of surface waves from explosions detonated in a wide variety of source materials (e.g., tuffs and granites at the Nevada Test Site).

A natural way to compare events in close proximity, but in different source materials, is to use two earth models, one for the source region and one for the remainder of the path. Alewine (1974) gives an approximate transmission coefficient to account for propagation of Rayleigh waves across a vertical boundary that is based on results given by McGarr (1969) and McGarr and Alsop (1967). Using this, the equation for explosion generated Rayleigh waves in a two-structure earth model is

$$\hat{w}(r,\omega) = - 4\Pi\mu_s \hat{\Psi}(\omega) \frac{K_{s_1} \tilde{A}_{R_1}}{c_1} T(\omega) H_o^{(2)} \left(\frac{\omega r_1}{c_1} + \frac{\omega r_2}{c_2}\right) \cdot$$

$$\exp\left(-\gamma_1 r_1 + \gamma_2 r_2\right) \left(\frac{r_1 + r_2}{a_e \sin(\Delta_1 + \Delta_2)}\right)^{1/2} . \quad (2.4)$$

where the source and receiver portions of the path are denoted by subscripts 1 and 2, respectively.

The transmission coefficient, $T(\omega)$, is derived by assuming the total horizontal energy flux remains constant during the transmission of Rayleigh waves across the boundary and is given by

$$T(\omega) = \left(\frac{c_2 \, A_{R_2}}{c_1 \, A_{R_1}}\right)^{1/2} . \quad (2.5)$$

The derivation of this coefficient assumes no mode conversion and includes no refraction effects.

For comparing events in close proximity like those at the Nevada Test Site (NTS), we should note the following points. First, as far as the generation of surface waves is concerned, the only difference between source structures occurs in the top few kilometers. Thus, for the long periods that are generally of primary interest, the boundary is nearly transparent and $T(\omega) \approx 1$. Second, it seems reasonable to let $r_1 \to 0$ because the dispersion and attenuation are average path quantities that, to the extent they are derived from events in the source region under study, already incorporate any mixed path effects that might be present. These points will be clarified by some examples in later sections.

Letting $r_1 \to 0$ in Equation (2.4), the formula to be used for computing the surface waves from underground explosions becomes

$$\hat{w}(r,\omega) = -4\Pi\mu_s \hat{\Psi}(\omega) \frac{K_{S_1} \underset{\sim}{A}_{R_1}}{c_1} T(\omega) H_o^{(2)}\left(\frac{\omega r}{c_2}\right) e^{-\gamma r} \left(\frac{r}{a_e \sin \Delta}\right)^{1/2} \tag{2.6}$$

where r is the range and the other quantities are as in Equation (2.5). With this formulation a single average path model can be used for all events in a region while accounting for changes in the local source material in a consistent way.

2.3 SURFACE WAVE DISPERSION FOR NTS-ALBUQUERQUE AND NTS-TUCSON

Data from the WWSSN stations ALQ and TUC were collected for a number of NTS explosions. A striking characteristic of these data was the consistency of the waveforms at each station. For example, the period of the maximum phase was measured for some 56 events recorded at ALQ and was found to be 11.0 $\pm$ 0.5 seconds. The analogous period for 59 events observed at TUC was 8 $\pm$ 0.5 seconds. Some typical examples are shown in Figure 2.1. The pertinent data for these events is summarized in Table 2.1 (from Springer and Kinnaman, 1971).

The path dispersion characteristics were determined by analysis of three representative recordings at each station. These events were in three geophysically distinct testing areas at NTS and their surface waves represent the range of variation seen at ALQ and TUC. The six seismograms were digitized by hand from reproductions of the WWSSN film chips.

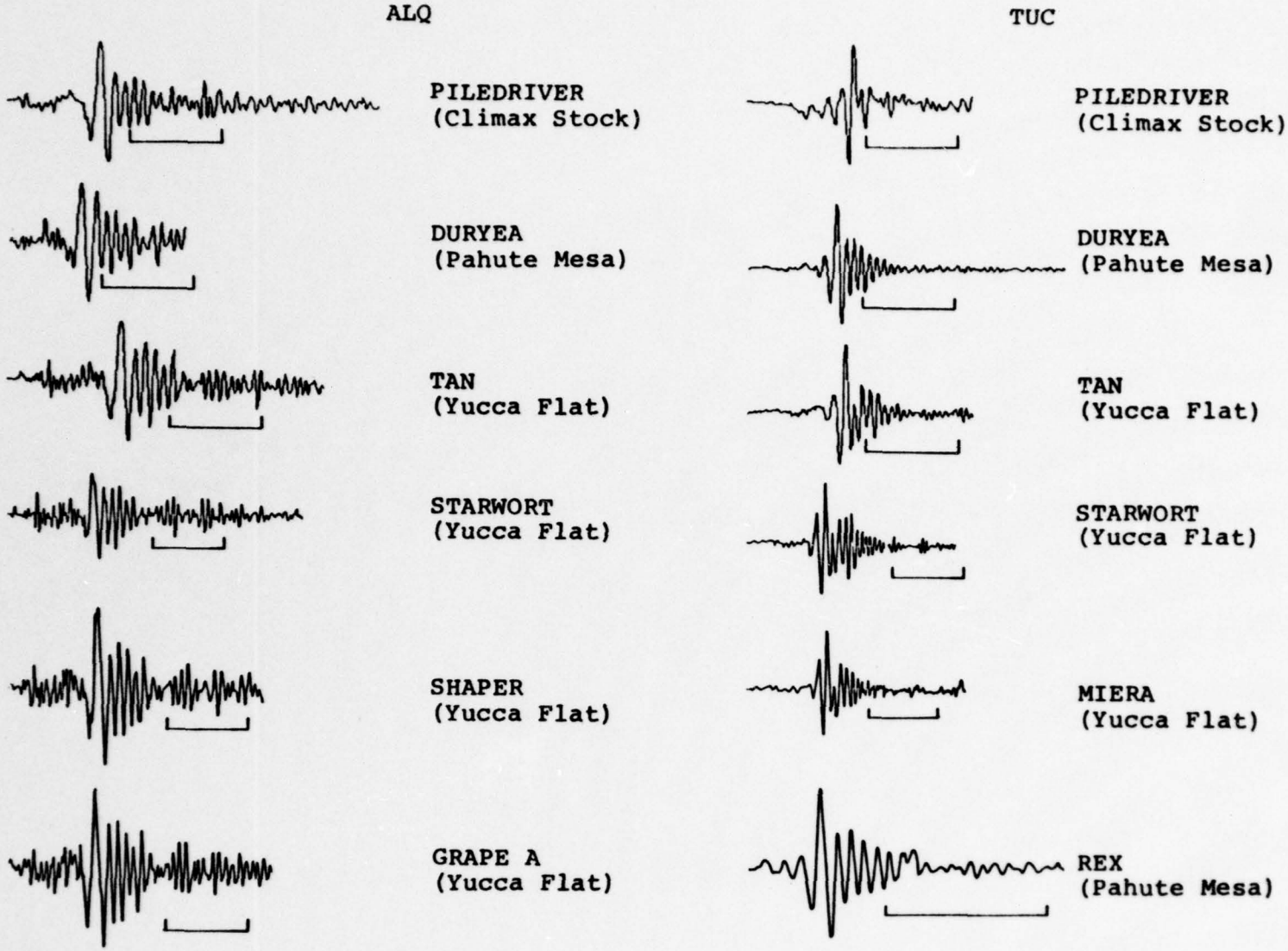

Figure 2.1. Typical seismograms are shown for six events recorded at each station. The first three events in each column are plotted from hand-digitized data while the others are tracings from the film records. All seismograms are not on the same time scale - one minute is indicated on each record.

TABLE 2.1

DESCRIPTION OF SELECTED EVENTS

Name and Date	Shot Time (GMT)	Yield (Kt)	Depth (km)	Source Area and Material	TUC Azimuth, Distance		ALQ Azimuth, Distance	
PILEDRIVER 6/2/66	1530:00:09	≈56	0.463	Climax Stock Granite	137°	728.1	103° 102°	900.4
TAN 6/3/66	1400:00:04	Low-Intermediate	0.544	Yucca Flat Tuff	136°	714.1	102°	894.7
DURYEA 4/14/66	1413:43:10	65	0.560	Pahute Mesa Rhyolite	135°	752.6	103°	933.2
STARWORT 4/26/73	1715:00:16	85	0.564	Yucca Flat Tuff	136°	719.9	103°	898.0
SHAPER 3/23/70	2305:00:04	Low-Intermediate	0.561	Yucca Flat Tuff	136°	714.7	103°	893.9
MIERA 3/8/73	1610:00:19	Low-Intermediate	0.569	Yucca Flat Tuff	136°	716.4	103°	894.8
GRAPE A 12/17/69	1500:00:04	Low-Intermediate	0.551	Yucca Flat Tuff	136°	713.3	103°	892.1
REX 2/24/66	1555:07:04	16	0.672	Pahute Mesa Tuff	135°	755.0	103°	934.2

The phase and group velocities for the seismograms of Figure 2.1 were determined using a program (Multiple Arrival Recognition System, MARS) developed primarily by Archambeau and described in numerous Systems, Science and Software contract reports (e.g., Bache, et al., 1976). In this program each seismogram is Fourier-transformed and filtered by a narrow-band, Gaussian filter. The inverse-transformed narrow-band output and its Hilbert transform are constructed to obtain the envelope as a function of time. The peaks of the envelope function occur at the group arrival times of energy in a narrow band of frequencies near the filter center frequency. Generally, the narrower the filter, the less the contamination by energy from adjacent frequencies, but the less accurate the arrival time determination. For this reason each seismogram was analyzed using several filter widths. The group velocity was then determined as a function of period for each seismogram, assuming zero group delay at the source. These data are plotted in Figure 2.2 together with the average group velocity for the two paths, NTS-TUC and NTS-ALQ, under study.

For determining earth structure, phase and group velocity together have considerably more resolving power than the group velocity alone. For recordings of explosions at these ranges the phase and group velocities seem to have about the same accuracy. Referring to Equation (2.6), the phase of the vertical component of the Rayleigh wave can be written $-\omega T$. Using the far-field approximation for the Hankel function, T is

$$T = T_s + \frac{r}{c_2} + \frac{3\Pi}{4\omega} \qquad (2.7)$$

where T_s is the phase delay associated with the source function $\dot{\Psi}(\omega)$. Theoretical (e.g., Bache, et al., 1975) and empirical

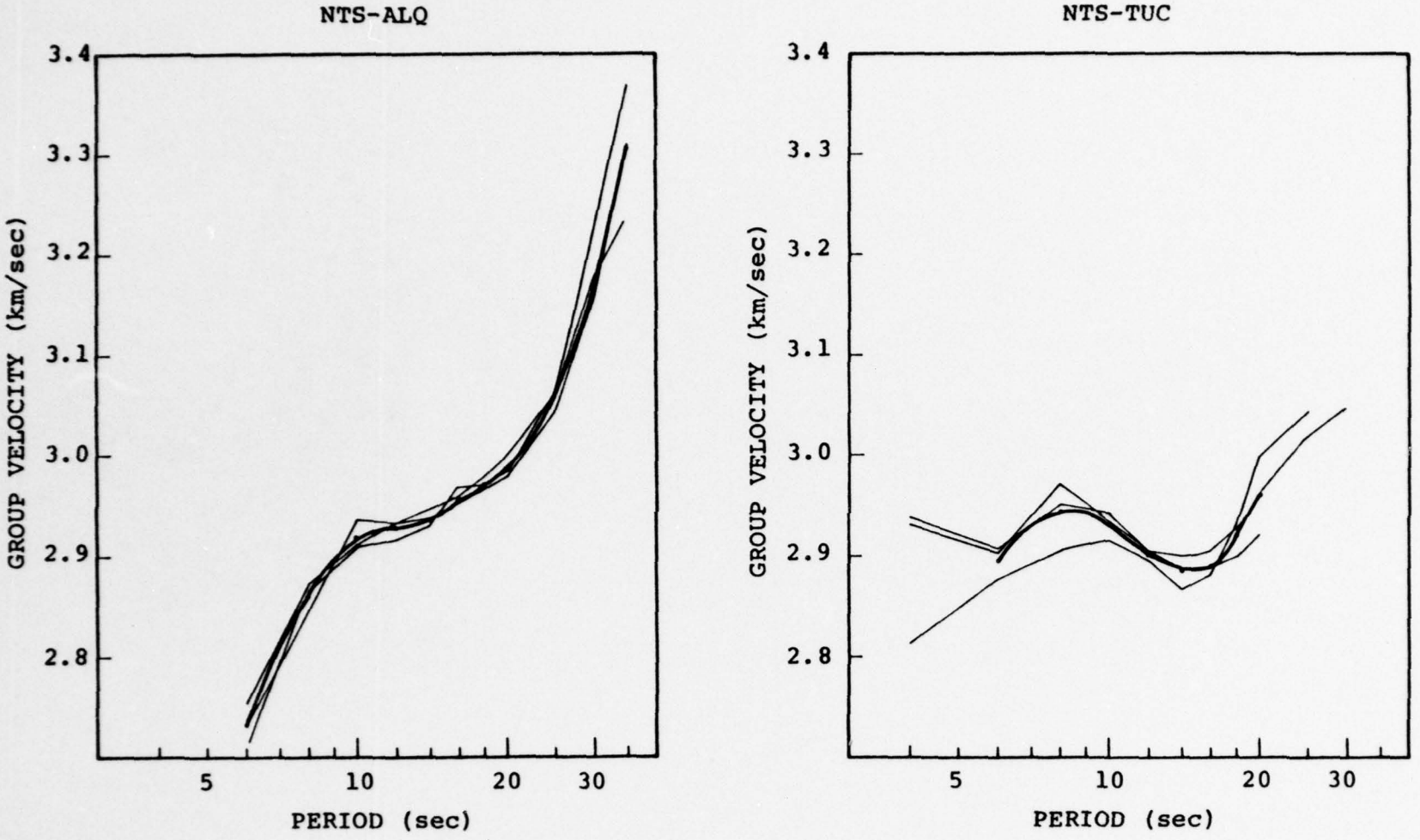

Figure 2.2. The group velocity is plotted for the two paths under study. The light lines are the values for the three seismograms analyzed at each station. The "average" values used for the inversion are indicated as open circles along the heavy lines.

(e.g., Haskell, 1967) studies of the source find T_s to be at most a few tenths of a second at periods in the range of interest so it can safely be ignored.

The phase velocities are determined in the following way. The phase of the Fourier-transformed seismogram is first unwrapped; that is, jumps of 2π are removed. Denoting the unwrapped phase by ϕ, we then solve for phase velocity from

$$c_2 = \frac{-r\omega}{\phi + \frac{3\pi}{4} + 2n\pi} , \tag{2.8}$$

where n is an integer selected to give reasonable values for c_2. The phase velocity data are plotted in Figure 2.3 together with the average values for each path. The phase velocities for n being $\pm$ 1 from the value chosen are also indicated. These phase velocities lead to unrealistic earth models.

Comparing the phase and group velocities, we see that they both are remarkably constant from event to event, especially for the NTS-ALQ path, and appear to provide equally accurate data sets. Since the phase and group velocities were determined using entirely different methods, an excellent check is the fact that they agree closely with the relationship

$$\frac{1}{U_2} = \frac{d}{d\omega}\left(\frac{\omega}{c_2}\right) \tag{2.9}$$

where U_2 is the group velocity.

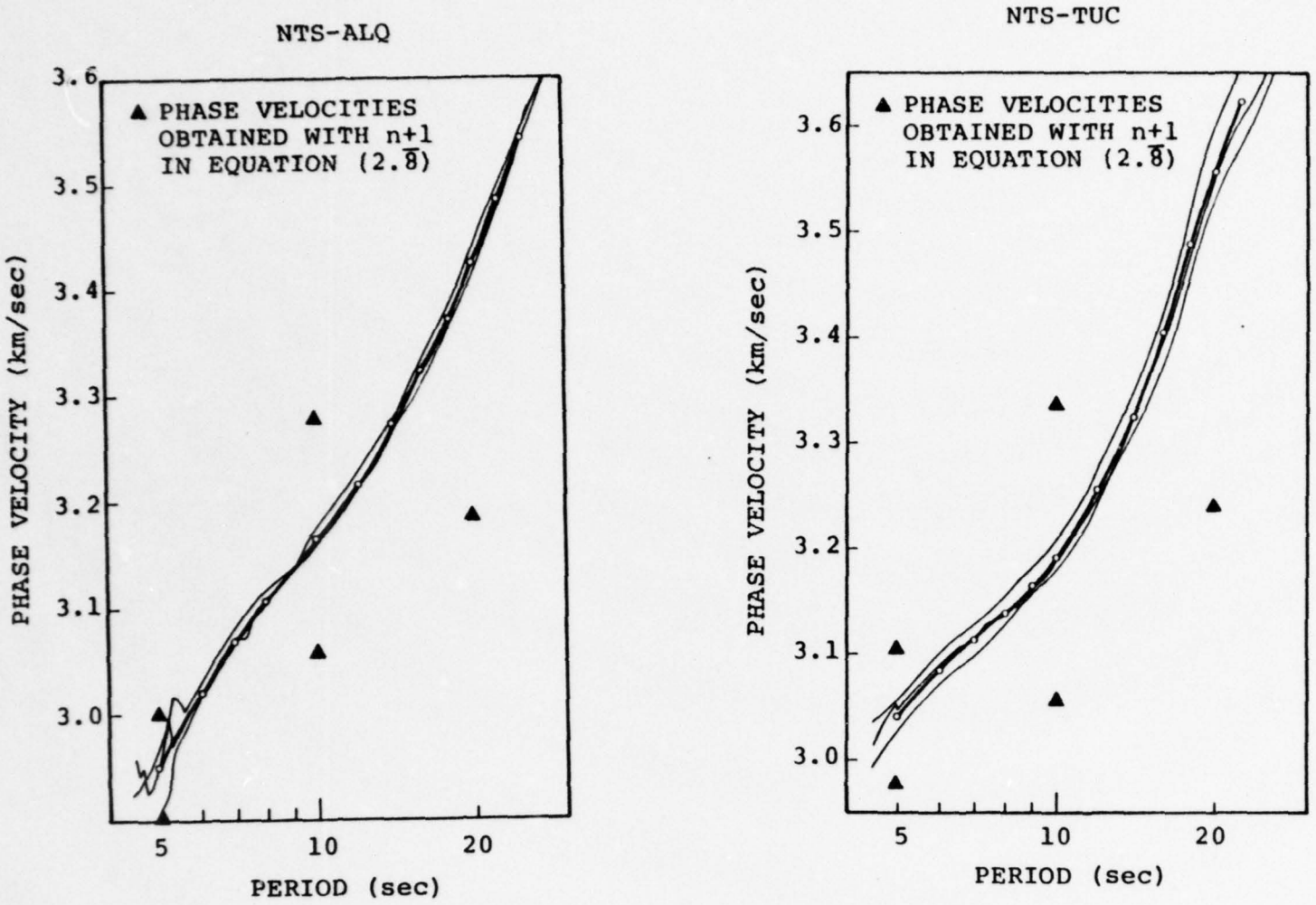

Figure 2.3. The phase velocity data are plotted in the same format as the group velocity data in Figure 2.2.

2.4 EARTH STRUCTURE FROM INVERSION OF SURFACE-WAVE PHASE AND GROUP VELOCITY

2.4.1 Method

Systematic linear inversion is the most effective available method for inferring the average earth structure along a surface-wave path from the observed dispersion. Given a set of phase and group velocities for a path, the method determines an optimal earth structure fitting these data and, at the same time, describes the resolving power of the data.

In our inversion, we assume that phase velocity and group velocity depend only on the depth variations of shear velocity β, compressional velocity α, and density ρ. The effects of lateral variations and inelasticity are not modeled. A set of M phase and group velocity data, d_i, $i = 1, \ldots, M$, is then related to earth structure by

$$d_i = D_i\big(\alpha(z), \beta(z), \rho(z)\big) + e_i, \quad i = 1, \ldots, M \quad , \tag{2.10}$$

where D_i is a functional that expresses the theoretical relationship between d_i and (α,β,ρ) and where e_i is the experimental error in d_i. Linear inversion finds a solution to Equation (2.10) in the form of a model $(\hat{\alpha}(z), \hat{\beta}(z), \hat{\rho}(z))$ which, in effect, is an estimate for spatial averages of (α,β,ρ).

One objective of inversion is to find a model whose dispersion agrees with the observed data within their experimental accuracy. Namely, we want $|d_i - \hat{d}_i|$ to be less than the standard deviation of e_i, where

$$\hat{d}_i = D_i\ (\hat{\alpha},\hat{\beta},\hat{\rho}) \ , \quad i = 1, \ldots, M \ . \tag{2.11}$$

Because of nonuniqueness, an infinite number of such models might exist, assuming the accuracy of the data is not overestimated and the theory expressed by D_i is accurate.

Therefore, a second objective is to find a model that is "smooth;" that is, one that is simple (few distinct layers) and consistent with other information about the path.

Linear inversion simultaneously maximizes smoothness and the fit to the observed data. An important task is formulating a mathematical smoothness criterion that neither eliminates desirable models nor admits undesirable models as solutions. Many smoothness criteria have been proposed and used in geophysical inverse problems (for example, Backus and Gilbert, 1970; Jordan, 1973; Wiggins, 1972; Gilbert and Johnson, 1972). The method used here is similar to previous methods but differs from them in some important respects. We describe the resulting inversion method briefly here and more fully in a topical report in preparation.

A limited number of fundamental-mode Rayleigh-wave phase and group velocities in a finite frequency band do not provide enough information to determine α, β, and ρ individually. The dependence on α and ρ is weak compared to the dependence on β, so α and ρ are often treated as known parameters in surface-wave inversion. To be less restrictive, we assume that α and ρ are linearly related to β and set

$$\hat{\alpha}(z) = C_{1\alpha}(z)\,\hat{\beta}(z) + C_{2\alpha}(z) \quad ,$$
$$\hat{\rho}(z) = C_{1\rho}(z)\,\hat{\beta}(z) + C_{2\rho}(z) \quad , \tag{2.12}$$

where $C_{1\alpha}$, $C_{2\alpha}$, $C_{1\rho}$, $C_{2\rho}$ are prescribed. This allows a great deal of flexibility that can be used to fix α, ρ, Poisson's ratio, or other functions of the model at various depths.

To find $\hat{\beta}$, we minimize the quantity χ, given by

$$\chi(\hat{\beta}) = \chi_1(\hat{\beta}) + \theta\chi_2(\hat{\beta}) \quad , \tag{2.13}$$

where χ_1 measures the fit to the data and is defined by

$$\chi_1(\hat{\beta}) = \sum_{i=1}^{M} (d_i - \hat{d}_i)^2 / \mathrm{Var}(d_i) \ , \tag{2.14}$$

and where χ_2 measures the unsmoothness of $\hat{\beta}$, which we define in the following way. The halfspace $z \geq 0$ is divided into S segments between which discontinuities in β are known or believed to exist. The segments are defined by $z_{s-1} \leq z \leq z_s$, $s = 1, \ldots, S$, where $z_o = 0$ and $z_S = \infty$. Then χ_2 is

$$\chi_2(\hat{\beta}) = \sum_{s=1}^{S} \int_{z_{s-1}}^{z_s} dz \left(\frac{d\hat{\beta}}{dz}\right)^2 \ . \tag{2.15}$$

This definition encourages $\hat{\beta}$ to be as smooth as possible between discontinuities but restricts neither the average value of $\hat{\beta}$ within each segment nor the jump in value across each discontinuity. The positive "tradeoff parameter" θ controls the relative importance of maximizing the fit to the data compared to maximizing smoothness.

To minimize χ, we must approximate the data functionals D_i with linear expansions about a reference model $(\alpha_o, \beta_o, \rho_o)$. This results in

$$\hat{d}_i = D_i\,(\alpha_o,\beta_o,\rho_o) + \int_o^\infty dz \left[G_{\alpha i}\,(\hat{\alpha}-\alpha_o) + G_{\beta i}\,(\hat{\beta}-\beta_o) + G_{\rho i}\,(\hat{\rho}-\rho_o) \right] + \text{second order terms}, \tag{2.16}$$

where $G_{\alpha i}(z)$, $G_{\beta i}(z)$, and $G_{\rho i}(z)$ are the differential kernels of D_i with respect to α, β, and ρ, respectively, evaluated at the reference model. Assuming $(\alpha_o,\beta_o,\rho_o)$ obeys Equation (2.12), Equation (2.16) can be written

$$\hat{d}_i = D_i\ (\alpha_o,\beta_o,\rho_o) + \int_o^\infty dz\ G_i(z)\ (\hat{\beta}-\beta_o)\ , \qquad (2.17)$$

where

$$G_i = G_{\beta i} + C_{l\alpha}\ G_{\alpha i} + C_{l\rho}\ G_{\rho i}\ . \qquad (2.18)$$

The model that minimizes χ, given Equations (2.13) through (2.18), is

$$\hat{\beta}(z) = \sum_{i=1}^{M} G_i^{+}(z) \left[d_i - D_i(\alpha_o,\beta_o,\rho_o) + \int_o^\infty dz\ G\beta_o \right], \qquad (2.19)$$

where the functions $G_i^{+}(z)$ represent a generalized inverse of the differential kernels $G_i(Z)$ and depend only on G_i, $Var(d_i)$, and the tradeoff parameter θ.

One advantage of this method compared to other methods is that $\hat{\beta}$ does not depend directly on the reference model, but only indirectly through the dependence of G_i on $(\alpha_o,\beta_o,\rho_o)$ due to the fact that the D_i are nonlinear functionals of (α,β,ρ). Because of this nonlinearity, it is often necessary to find $\hat{\beta}$ iteratively by repeating Equation (2.19) one or more times with $(\alpha_o,\beta_o,\rho_o)$ replaced by the model obtained from the previous iterate.

The uniqueness of $\hat{\beta}$ is described by the relationship between $\hat{\beta}$ and β, obtained by substituting Equation (2.10) into Equation (2.19):

$$\hat{\beta}(z) = \int_o^\infty dz' A(z,z')\ \beta\ (z') + \varepsilon(z)\ ,$$

$$A(z,z') = \sum_{i=1}^{M} G_i^{+}(z)\ G_i(z')\ , \qquad (2.20)$$

$$\varepsilon(z) = \sum_{i=1}^{M} G_i^{+}(z)\ e_i\ .$$

This states that $\hat{\beta}(z)$ is an estimate for a weighted spatial average of $\beta(z)$ for which the error of estimation is $\varepsilon(z)$. The variance of $\varepsilon(z)$ can be obtained directly in terms of the variance of the data. For a given depth z, the width of the "averaging kernel," $A(z,z')$, with respect to z' describes the scale of the most detailed feature that the data can resolve with variance $\mathrm{Var}(\varepsilon(Z))$.

The numerical implementation of this method requires that an earth model be described by a finite discrete set of parameters rather than continuous functions of depth. Therefore, models with a finite number of plane horizontal homogeneous layers are used. In the discrete analog of the method, integrals are replaced by summations and the differential kernels are replaced by the partial derivatives of phase and group velocity with respect to layer parameters. The functionals D_i are evaluated by the method described by Harkrider (1964). With this technique, exact phase velocity partial derivatives can be expressed in terms of energy integrals (Takeuchi, et al., 1962). Approximate but accurate group velocity partial derivatives are obtained by a numerical scheme due to Rodi, et al., (1975).

2.4.2 Inversion for the NTS-TUC and NTS-ALQ Paths

An acceptable model of the earth's structure must satisfy other data about the region as well as our phase and group velocity data. The NTS-TUC path, in particular, has been studied by others and some of the main features of the crust are fairly well known. While much less work has been done along the NTS-ALQ path, there are some good data that should not be violated. These data and other information about the character of the crust are used to guide the inversion. First, they are used to select values for the parameters

$C_{1\alpha}$, $C_{2\alpha}$, $C_{1\rho}$ and $C_{2\rho}$ in Equation (2.12). Further, the refraction data help to locate the major discontinuities, especially the crust-mantle boundary.

A number of previous studies have suggested models for the crust along the NTS-TUC path. Refraction lines have been run along much of this path and have been studied by Diment, et al., (1961) and Langston and Helmberger (1974). The latter study used both amplitude and travel-time information from the refraction seismograms and supplemented this with group velocity dispersion determined from TUC surface wave recordings of NTS explosions. The authors concluded that the crust was about 30 km thick and relatively uniform with α = 6.1 km/sec, β = 3.6 km/sec except for a 1 km sedimentary layer at the surface. The P_n velocity was 7.9 km/sec, a typical value for the Basin and Range Province.

Warren (1969) used refraction data to derive a model for central Arizona that is in basic agreement with that of Langston and Helmberger. He found the crustal thickness to increase from 21 km in southwest Arizona to 40 km in northeast Arizona, with the thickness being about 30 km where the profile crosses the NTS-TUC path. His model differs from that of Langston and Helmberger in having a high velocity (α = 7 km/sec) layer at the base of the crust.

Data for the NTS-ALQ path is less abundant, though there is agreement that the crustal thickness gets generally greater from west to east. Prodehl (1970) used refraction data and found a thickening crust from 30 km near NTS to over 40 km in north-central Arizona. He found P_n velocities between 7.6 and 7.9 km/sec in northern Arizona. Using data from a north-south refraction profile in central New Mexico, Toppozada and Sanford (1976) concluded that the crust was about 40 km thick, with a P_n velocity of 7.9 km/sec. Keller, et al., (1976) inverted for structure in the Colorado Plateau, northeast of NTS, from

Rayleigh wave group velocity data. They found a 40 km crust with β increasing from 3.5 km/sec at 2 km depth to 3.9 km/sec at the base of the crust.

Taking account of these other data, our starting model for the inversion of the phase and group velocities was constrained to have a low velocity sedimentary layer at the surface and a crust-mantle boundary at a specified depth. Poisson's ratio (ν) was fixed in the crust as were the α and ρ in the mantle. These constraints are summarized in Table 2.2.

How strongly do our models depend on the constraints in Table 2.2? First, the dispersion data are primarily controlled by β so the α-β and ρ-β relationships do not greatly affect the ability of the inversion to find a model that fits the data. They serve mainly to guarantee a self-consistent model. Since our shortest period data are at 5 seconds, the data are also fairly insensitive to the sedimentary layer. The constraint most important to fitting the data is the crustal thickness. Trial inversions with crustal thicknesses much different from those in Table 2.2 gave models that were unable to fit the dispersion data as well and/or gave unacceptable values for the mantle velocity. Certainly the dispersion data could be fit with a smooth crust-mantle transition, but this would deny the existence of a P_n refractor.

The models inverted from the data are shown in Figures 2.4 and 2.5, together with a comparison of model phase and group velocities to the observations. In both cases the final model was obtained with two iterations. Clearly, the models are in excellent agreement with the observed dispersion data; the largest residual is 0.01 km/sec. Further, these models are compatible with the refraction data where it is available. However, we should point out that the refraction studies primarily determine the P velocity while our study primarily determines shear velocity.

TABLE 2.2

CONSTRAINTS IMPOSED ON THE INVERSION

	ALQ	TUC
Sediment Thickness:	2.5 km	2.0
Crustal Thickness:	42.0 km	31.0
Crust:	$\alpha = 1.695\beta$ ($\nu = 0.23$) $\rho = 0.273\beta + 1.815$	
Mantle:	$\alpha = 7.9$ km/sec $\rho = 3.2$ gm/cm^3	

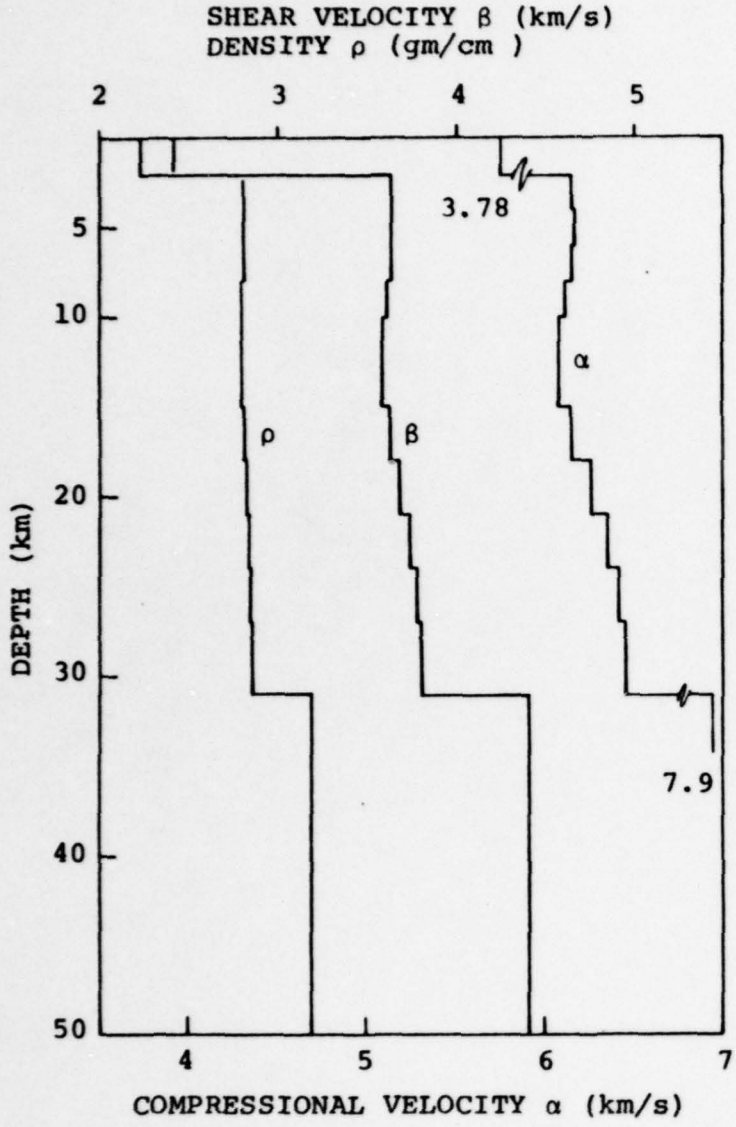

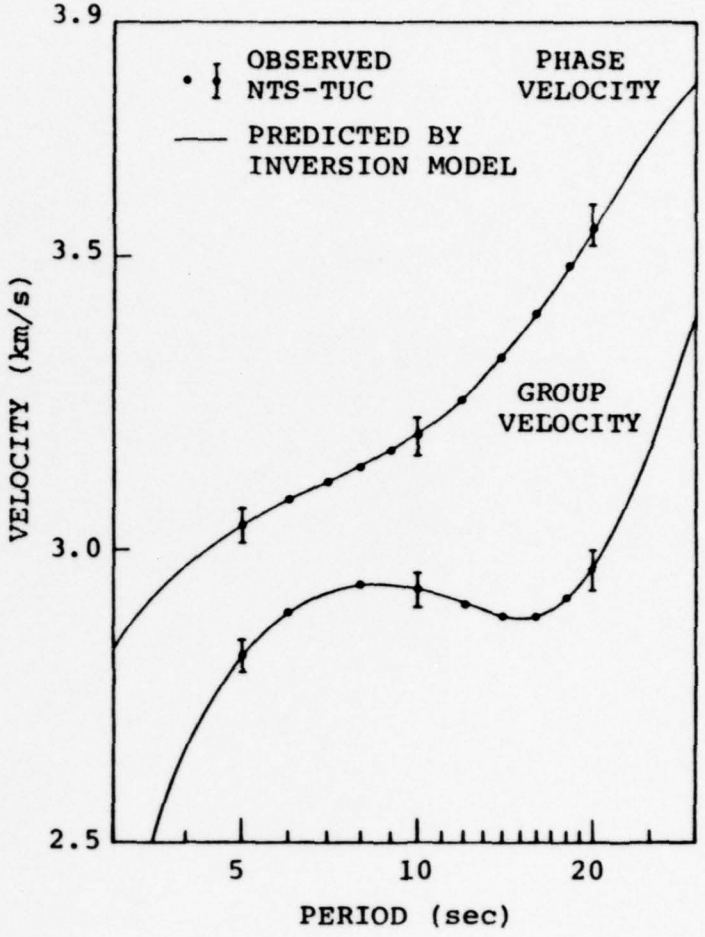

Figure 2.4. The inversion model (left) for the NTS-TUC path is shown together with a comparison of the observed data and model dispersion. The error bars at 5, 10 and 20 seconds on the dispersion plot denote one percent deviations from the observed data.

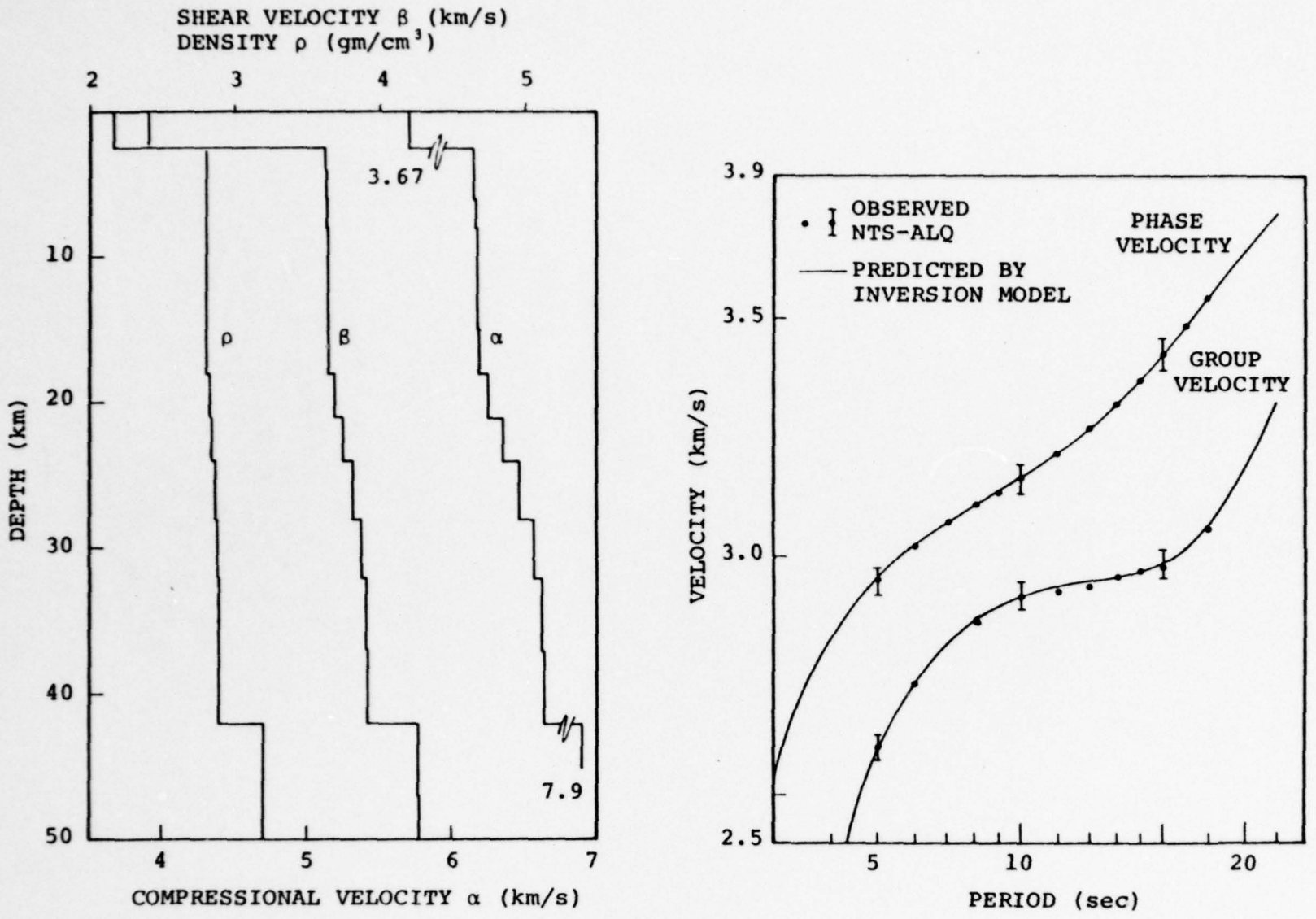

Figure 2.5. The inversion model and dispersion comparison is shown for the NTS-ALQ path in the same format as in Figure 2.4.

An attractive feature of the inversion models is their simplicity. In fact, four-layer models would fit the data very well. The best-resolved portion of the model is that between 5 and 20 kilometers. In this region our estimate for β is actually an average value over 6 km intervals and is determined to approximately one percent (assuming the data are accurate to one percent). This resolving power is not enough to make the slight velocity minimum at 12 km in the NTS-TUC model a significant feature. Also, the upper few kilometers of each model are poorly resolved, so the thickness and properties of this layer are not well-determined.

While it is difficult to resolve, a Conrad discontinuity in the NTS-ALQ model is suggested by the velocity increase from 3.64 km/sec at 15 km to 3.91 km/sec at 42 km. However, the gradual increase found by the inversion is an equally plausible feature. For the NTS-TUC path there is less suggestion of a Conrad discontinuity.

A difficulty with interpreting the NTS-ALQ model is the evidence (from refraction studies) for a strong east-west variation in crustal thickness. The crustal thickness of our plane-layered model represents in some way an average of this lateral variation. A number of trial inversions were done with different crustal thicknesses and a tradeoff between crustal thickness and upper mantle shear velocity was found. A thin crust, say 35 km, results in an unreasonably low mantle shear velocity. On the other hand, a crustal thickness of 45 km or more gives a more reasonable mantle shear velocity, but seems too thick to be the average thickness for this path. The value chosen, 42 km, was judged best, though thicknesses a few kilometers different can also be justified.

Since the inversion determines the mantle shear velocity while the refraction data was used to fix the mantle P velocity, the mantle Poisson's ratio is a result of the inversion. Our

mantle shear velocities are somewhat lower than those in other models (e.g., Langston and Helmberger, 1974), but still imply reasonable Poisson's ratios. For the NTS-TUC path β = 4.4 km/sec, ν = 0.27 in the topmost mantle. The analogous values for the NTS-ALQ mantle are 4.27 km/sec and 0.29.

2.5 CALCULATION OF THEORETICAL SEISMOGRAMS

Using the earth models of the previous section and Equation (2.6) we now calculate theoretical seismograms for comparison to the observations. The model for the NTS-TUC path is thought to be the more appropriate for NTS, primarily because of its relatively thin crust. Therefore, for the source region we use this model and change the top two kilometers to represent the specific test area (Climax Stock, Pahute Mesa or Yucca Flat). The velocity-depth profile for this portion of the model is shown in Figure 2.6.

Referring to Equation (2.6), the Rayleigh waves from explosions in different source materials are proportional to

$$\mu_s \hat{\Psi}(\omega) \frac{K_{s_1} \underset{\sim}{A}_{R_1}}{c_1} T(\omega) . \qquad (2.20)$$

For the periods ($T > 4$ seconds) and yields ($50 < W < 500$ kt) of interest, $\hat{\Psi}(\omega)$ is essentially equal to a constant, Ψ_∞, which represents the source coupling into elastic waves and depends on the local rock properties (e.g., Haskell, 1967; Bache, et al., 1975). Aside from this coupling term, the source excitation is then given by $\mu_s K_{s_1} \underset{\sim}{A}_{R_1} / c_1$ and is plotted in Figure 2.7 for the three test areas. The other quantity in Equation (2.20), $T(\omega)$, is plotted in Figure 2.8 for the six source-path structure combinations. The $T(\omega)$ is intended to represent, albeit approximately, the transmission of Rayleigh waves from the

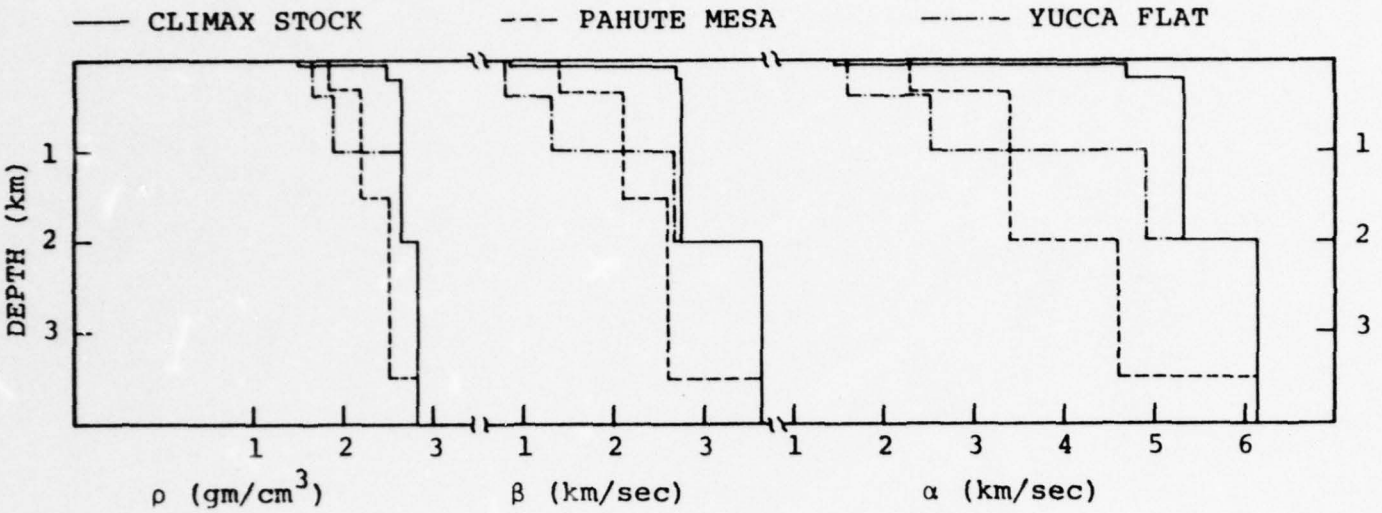

Figure 2.6. The density, shear and compressional wave velocities are plotted versus depth for the three test areas at NTS. Below 3.5 km the source region models are the same as the NTS-TUC model in Figure 2.4.

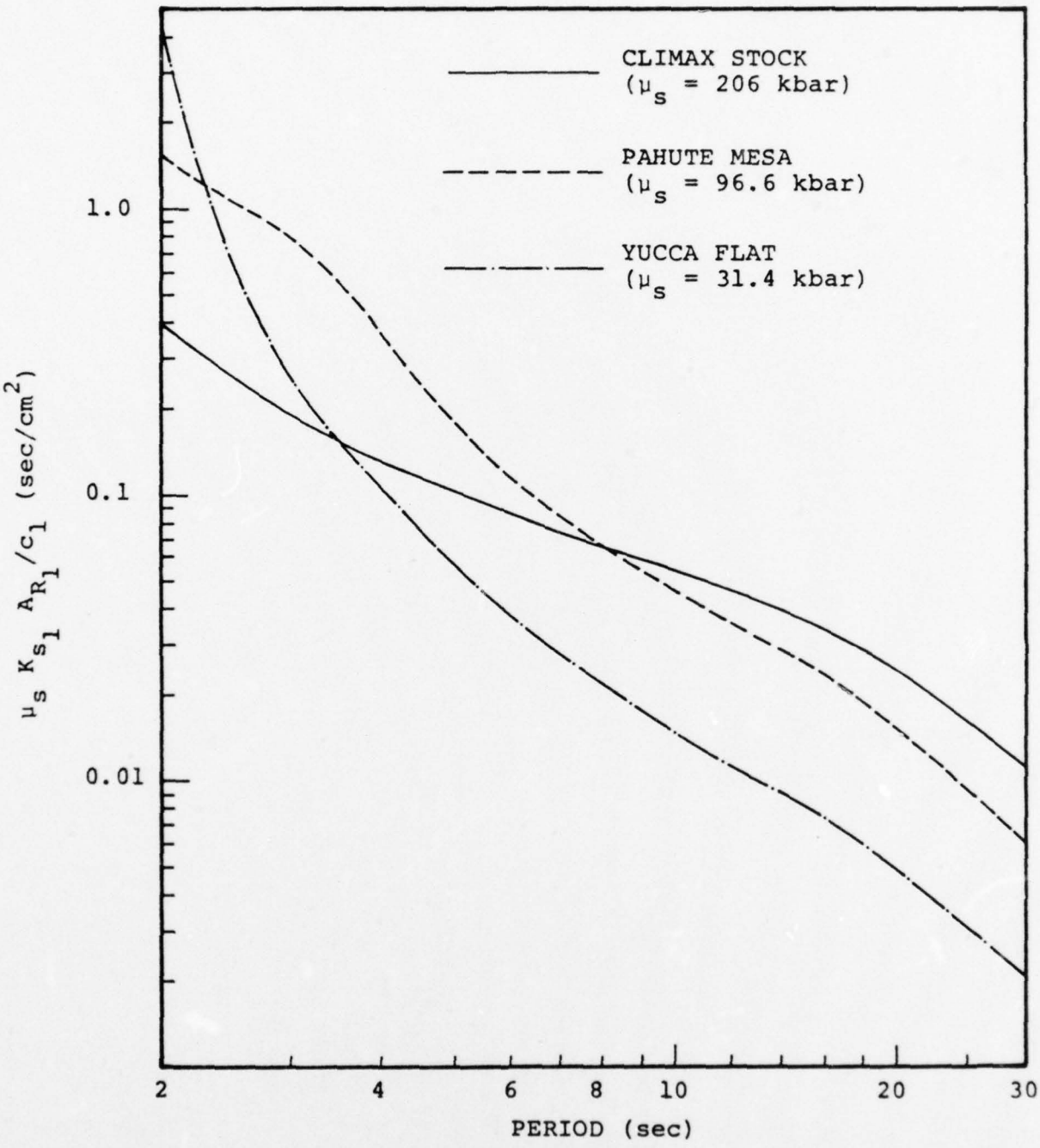

Figure 2.7. The source amplification factor is shown for the three source areas studied.

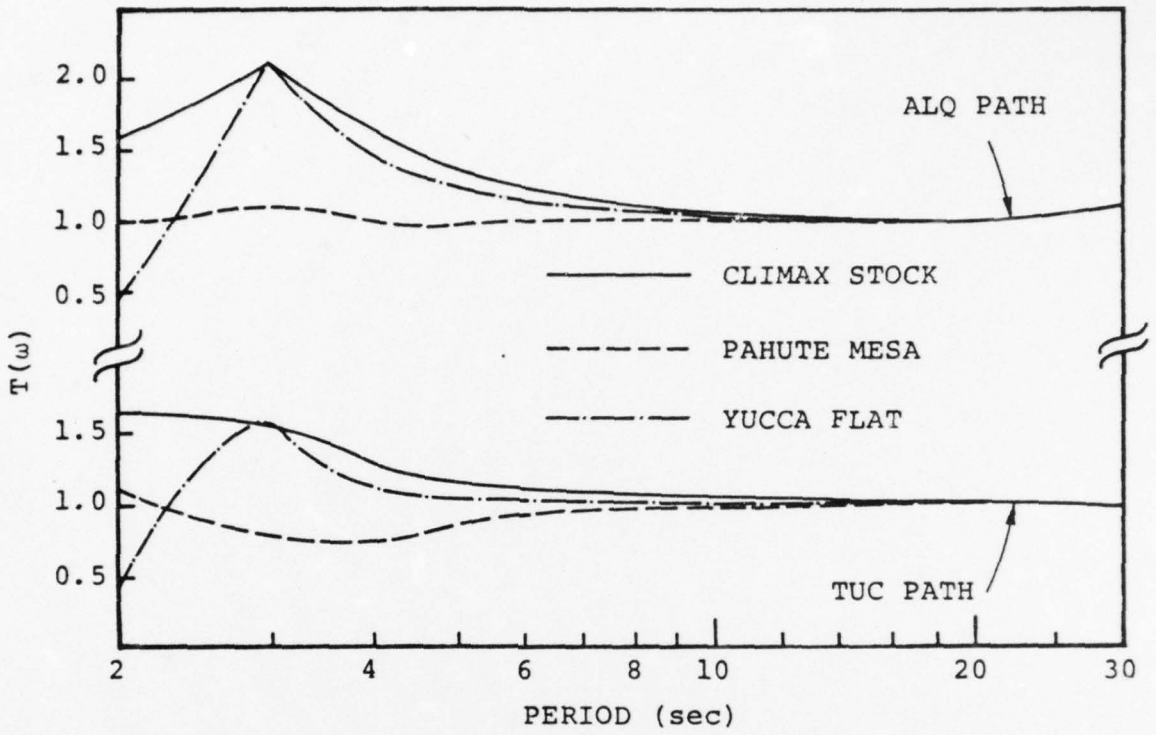

Figure 2.8. The transmission coefficient $T(\omega)$ is plotted for the six source-path combinations studied.

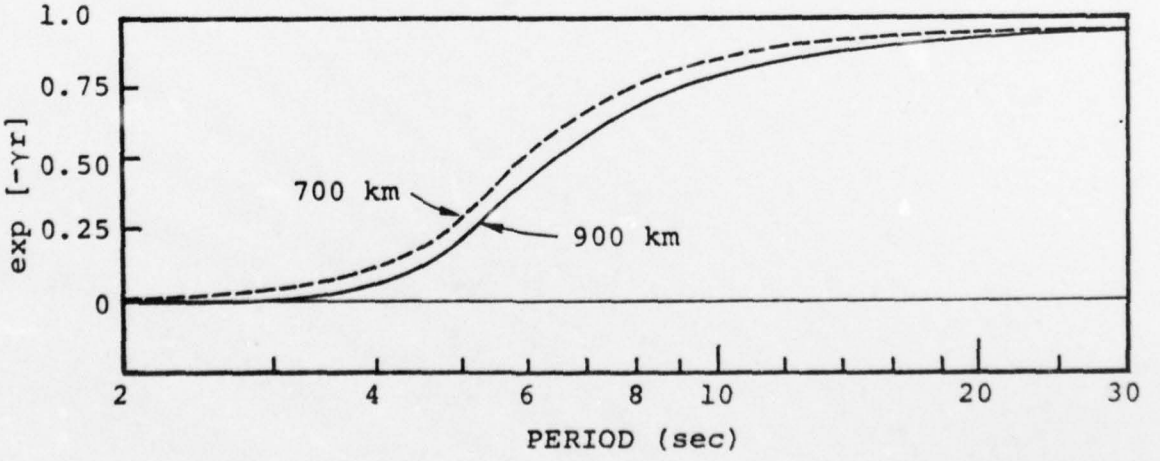

Figure 2.9. The amplitude attenuation due to the chosen $\gamma(\omega)$ is plotted for the NTS-TUC ($r \approx 700$ km) and NTS-ALQ ($r \approx 900$ km) paths.

source model to the path model. In Figure 2.8 we see that $T(\omega) = 1.0 \pm 0.15$, for periods greater than 5 seconds for most of the paths. The exceptions, which are not severe, are for the ALQ path where the source and path models are quite different. Where the $T(\omega)$ deviates substantially from unity, it is at least qualitatively correct, amplifying the waves generated in the high velocity material and vice versa.

The relative source excitation terms (Figure 2.7) for Pahute Mesa and Yucca Flat differ by a constant factor over most of the frequency range. This constant is essentially the ratio of the shear moduli, the μ_s, for the two regions. On the other hand, the excitation function in the granite structure has a different period dependence and for the range plotted is much smaller than expected from the ratio of the shear moduli.

To complete the computation of theoretical seismograms, it is necessary to specify a Q or γ model. The model used is based on that described by Mitchell (1976). The attenuation, $\exp[-\gamma r]$, for 700 and 900 km is shown in Figure 2.9. For example, the attenuation at the period (11 seconds) of the maximum phase at ALQ is 0.86 and at TUC (8 seconds) it is 0.70. The attenuation factor must represent scattering losses as well as anelastic attenuation and at short periods, say $T \leq 5$ seconds, one might expect large scattering effects. Certainly the observed seismograms have little energy at periods below 5 seconds. For these reasons large γ values were used at the short periods.

2.6 COMPARISON OF THEORETICAL OBSERVED SEISMOGRAMS

The theoretical seismograms for these events are compared to the ALQ and TUC observations in Figure 2.10. The waveform agreement is remarkably good for all six events, even down to some rather subtle details. Deviation between

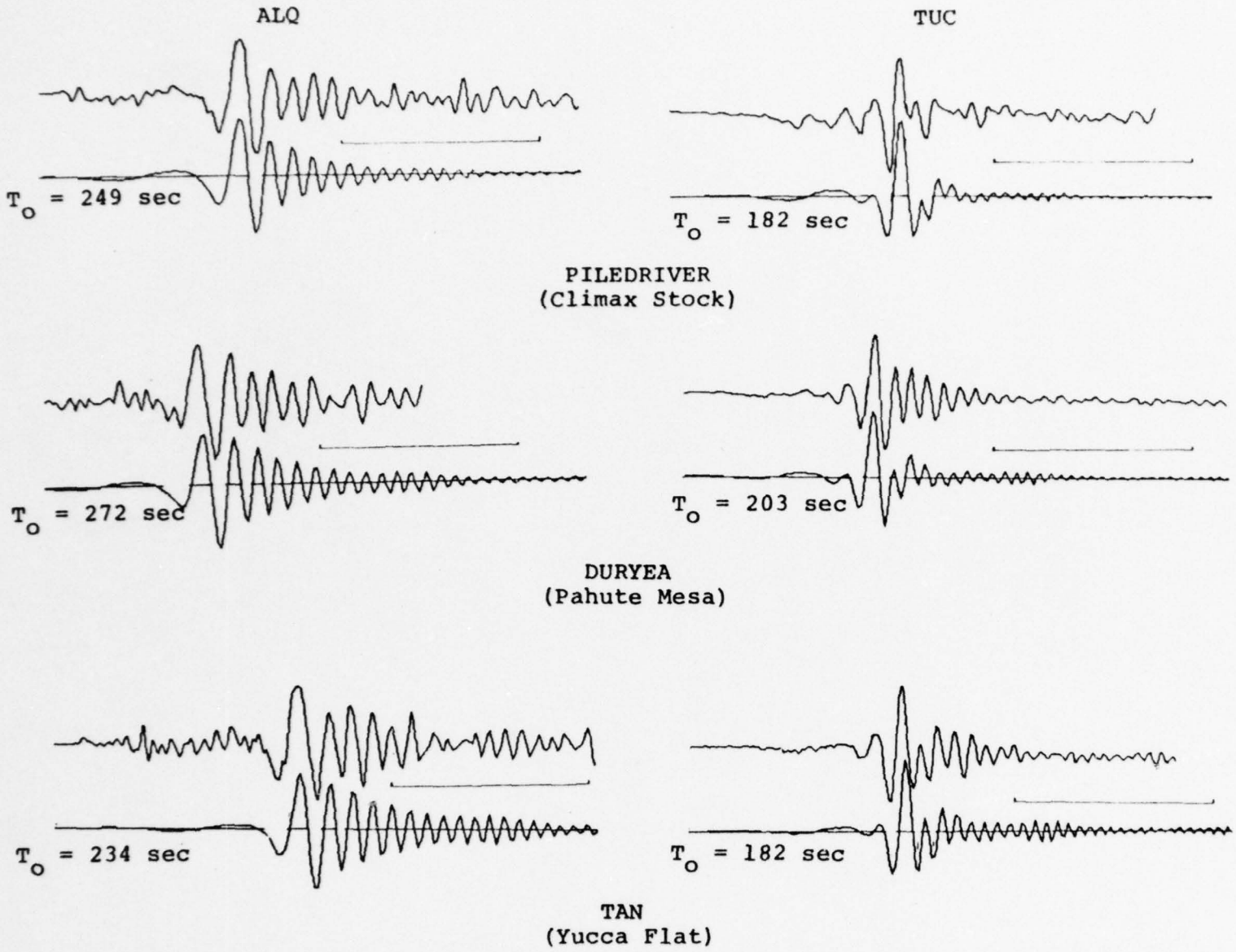

Figure 2.10. Theoretical and observed seismograms are compared at ALQ (left) and TUC for events in three test areas at NTS. A bar indicating one minute is shown. In each pair the observed and theoretical records start at the same time with respect to the explosion detonation and this time is indicated as T_o.

the two is either at periods (< 5 seconds) for which we could not extract dispersion data or, for ALQ, before the main pulse where there is coherent energy that may be a higher mode Rayleigh wave. This comparison is the final check on the consistency of our approach.

2.7 CONCLUDING REMARKS

The main features of this study can be quickly summarized. We collected a large number of recordings of NTS explosions at two WWSSN stations, ALQ and TUC. At each station the waveforms were found to be quite consistent. For an event in each of three test areas the records were digitized and analyzed for phase and group velocities. The phase velocity determination was by a straightforward unwrapping of the phase spectrum of the entire seismogram plotted in Figure 2.1. No special windowing was found to be necessary. The group velocities were determined by a more sophisticated approach relying on the Hilbert transform envelope of the narrow-band filtered seismogram. The two sets of data were entirely consistent and varied little from event to event.

Using an average phase and group velocity curve for each path, a linear inversion was done to determine the earth structure for the two paths. Models were found that gave agreement to the dispersion data with a maximum error of 0.01 km/sec. Further, these models are consistent with other available information on these paths, including that from refraction studies.

As a final check on the models, synthetic seismograms were compared to the observations and the two were found to be in remarkable agreement. Thus our models quite accurately account for the propagation of surface waves along these paths. Within the resolving power of the data and the restrictions imposed by the assumption of plane layers, the crustal structures in the regions sampled by the two paths must then closely resemble our models.

III. SMALL-SCALE LABORATORY SIMULATIONS OF EXPLOSION PRODUCED BODY WAVES - IMPLICATIONS FOR THE TELESEISMIC SIGNATURES OF UNDERGROUND NUCLEAR EXPLOSIONS

3.1 INTRODUCTION

In previous reports (Bache, et al., 1977; Barker, et al., 1977) we have described a series of small-scale laboratory experiments directed toward developing an improved understanding of the effect of depth of burial on the seismic signatures of underground nuclear explosions. In those experiments small spherical charges (0.25 gm of PETN) were detonated in grout cylinders. The displacement time histories were recorded on the flat surface of the cylinder farthest removed from the charge. Gauges were positioned at three points on this surface and the charges were detonated directly below one of these points. The experimental configuration is illustrated in Figure 3.1.

There were two distinct classes of experiments. In the first class the charges were emplaced in the center of the grout block. In this class of experiments the ground motion is uncontaminated by free surface reflected waves and is therefore free-field. In the second class of experiments the charge was detonated near the free surface and the direct P and free surface reflected pP are both present in the displacement histories. The latter class includes explosions at two burial depths; one in which the charges cratered and one in which they did not.

The most striking feature of the experimental data is a large negative pulse that occurs at late times (after the arrival of the pP phase) in the experiments in which free surface effects are present. Pulses of the same type were noted in full-scale nuclear cratering calculations carried out by Dr. J. Trulio at Applied Theory, Inc. (discussed by Dr. Trulio at several ARPA meetings in 1976-1977). What effect can a pulse of this kind

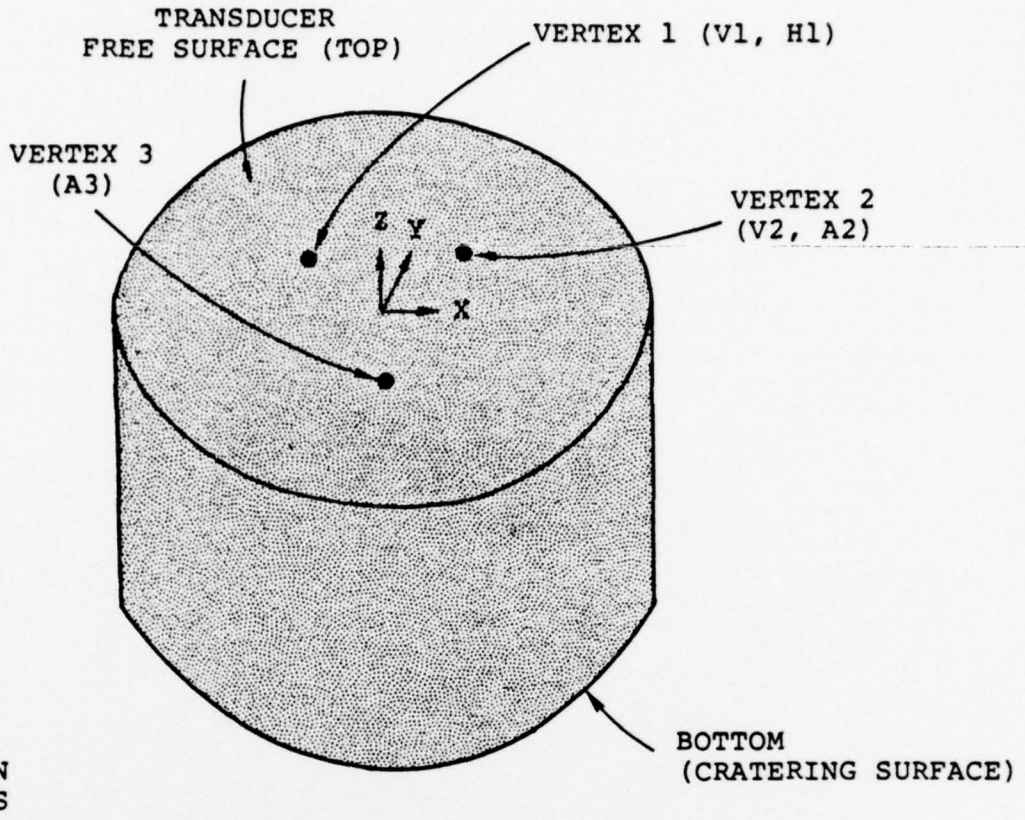

POINT	COORDINATES (X,Y,Z) cm
Vertex 1	(-15.2, 8.7, 0)
Vertex 2	(15.2, 8.7, 0)
Vertex 3	(0, -17.6, 0)
V1, Vertical Displacement Gauge	(-14.0, 8.7, 0)
H1, Horizontal Displacement Gauge	(-16.5, 8.7, -0.5) Sensitive axis || x
V2, Vertical Displacement Gauge	(14.0, 8.7, 0)
A2, Vertical Accelerometer	(16.5, 8.7, 0)
A3, Vertical Accelerometer	(0, -17.6, 0)
Charge 1	(-15.2, 8.7, -31)
Charge 2	(15.2, 8.7, -31)
Charge 3	(0, -17.6, -31)
Cylinder Bottom	(X, Y, -33 or -37 or -60 [Table I])

Figure 3.1. Schematic of the laboratory model. The diameter of the cylinder was 122 cm.

have on the teleseismic body wave signature of nuclear explosions? Further, how might it change the m_b-log yield relationship? This report addresses these questions.

If nuclear explosions have a large, late-arriving negative pulse like that seen in the experimental data, we conclude that it will significantly lower the slope of the m_b-log yield relation. The analysis leading to that conclusion is presented in the following sections. We first (Section 3.2) discuss the experimental data. In Section 3.3 an approximate equivalent elastic source representation is derived for each experiment. These sources are compared to typical theoretical source representations for nuclear explosions in Section 3.4. To study the implications of our experimental results for nuclear explosion signatures, it is necessary to scale them into the same frequency range. We find that elementary cube-root scaling provides a quite reasonable means to do so. Finally, in Section 3.5 we present our results in the form of synthetic seismograms and the m_b-yield data taken from these seismograms.

3.2 DISPLACEMENT TIME HISTORIES

The pertinent data describing the ten experiments that were done are summarized in Table 3.1. We see that there were four free-field experiments and six others, three of which cratered. As described in Figure 3.1, each charge was recorded by five gauges. In the ensuing analysis, we will be using the data from the displacement gauges emplaced on the normal from the charge to the free surface. There are no such data for Tests 3, 6 and 9, which were detonated in line with Vertex 3, and these tests will not be analyzed.

TABLE 3.1

SUMMARY OF DETAILS FOR SEISMIC MODELING EXPERIMENTS

Test No.	Cylinder Thickness (cm)	Distance to Nearest Free Surface (cm)	Distance of Charge Below Gauge (cm)	Crater Surface Dimensions (cm x cm)	Peak Displacement (μm)
0*	60	29.5 (Free-field)	30.5	-	4.5, 5.0, 6.7
1	37	6.5 (Underburied)	30.5 Vertex 1	-	5.3
2	37	6.5 (Underburied)	30.5 Vertex 2	-	3.5
3	37	6.5 (Underburied)	30.5 Vertex 3	-	5.5
4	60	29.5 (Free-field)	30.5 Vertex 1	-	4.9
5	60	29.5 (Free-field)	30.5 Vertex 2	-	3.3
6	60	29.5 (Free-field)	30.5 Vertex 3	-	3.1
7	33	1.75 ± 0.08 (Underburied, Crater)	31.3 Vertex 1	7 x 10	7.0
8	33	1.43 (Underburied, Crater)	31.6 Vertex 2	6 x 7	4.9
9	33	1.91 (Underburied, Crater)	31.1 Vertex 3	9 x 11	8.5

*Instrument Check

In Figure 3.2 data from the three free-field tests are plotted. Test 0 was different from the others in that two displacement gauges were placed together to check the gauge consistency. Therefore, in Figure 3.2 there are two records from Test 0 and one each from Tests 4 and 5. There is some indication that the gauge emplacement was bad in Test 5 and this record will be ignored. The other three time histories are in fairly close agreement in terms of peak and static displacements and the shape of the pulse. The time history from Test 4 will be used to represent the free-field displacement.

As another indication of the repeatibility of the direct P wave from the spherical charge, we compare the records from Tests 4 and 8 in Figure 3.3. Test 8 was one that cratered. A dramatic difference between the two is the large negative pulse in the cratering record. This is apparently due to the effect of the nearby free surface and we will say more about it below.

In Figure 3.4 we show the displacement time-histories from the five experiments to be compared. The free-field data is from Test 4 and the data from the contained and cratering experiments is from Tests 1, 2, 7 and 8; those for which we had recorded displacement time-histories along the normal between the charge and the free surface.

The grout was found to have a P wave velocity of about 3.38×10^5 cm/sec. Using this velocity and the distance to the nearby free surface (Table 3.1), we can calculate a theoretical elastic P-pP lag time. Using this, the expected arrival time of the free surface reflected pP wave is indicated on the time histories in Figure 3.4. For the contained experiments the pP wave is seen at about the right time. But it is followed by another negative pulse that cannot be explained with elastic theory.

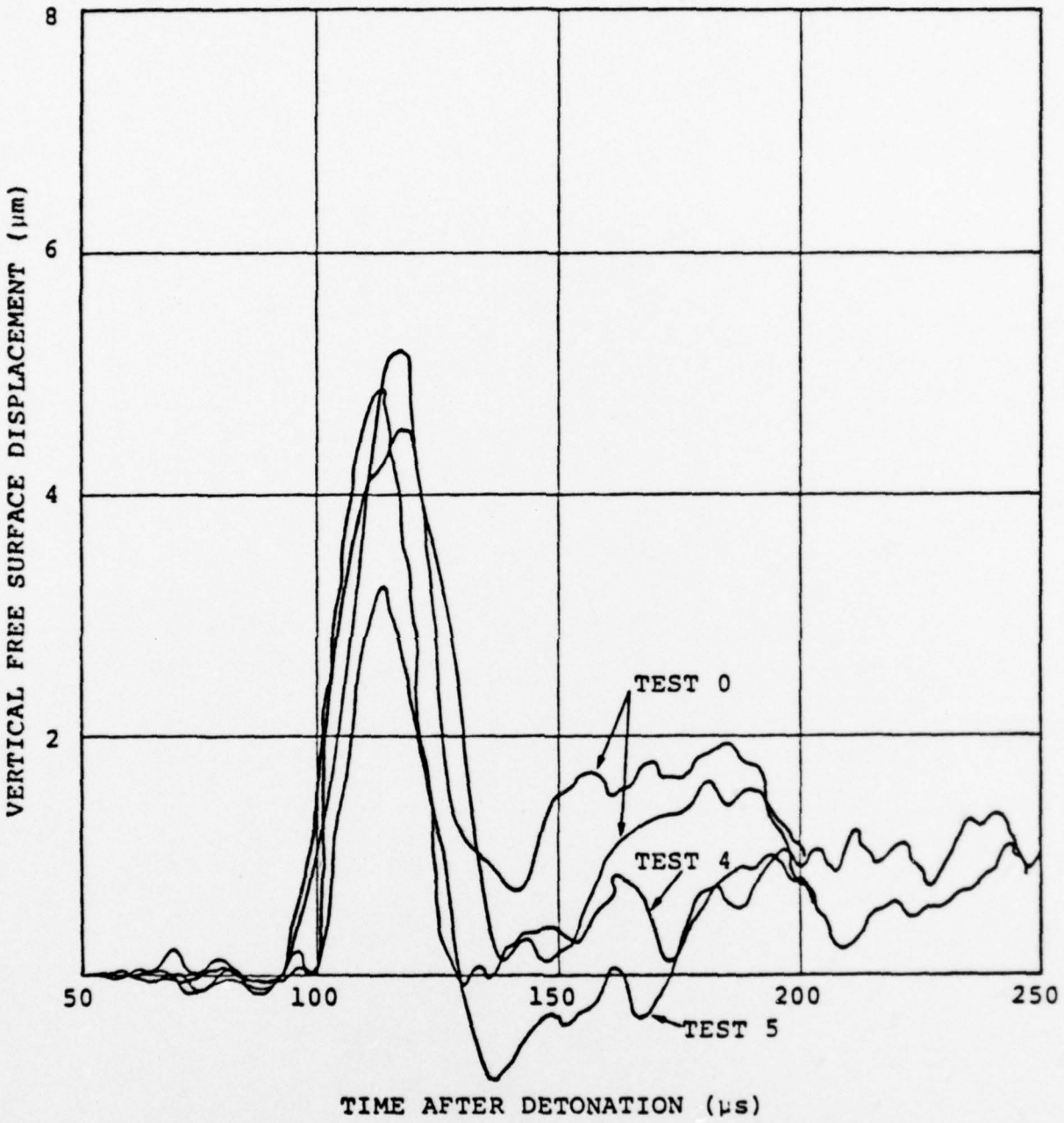

Figure 3.2. Displacement-time histories are plotted for the three free-field experiments.

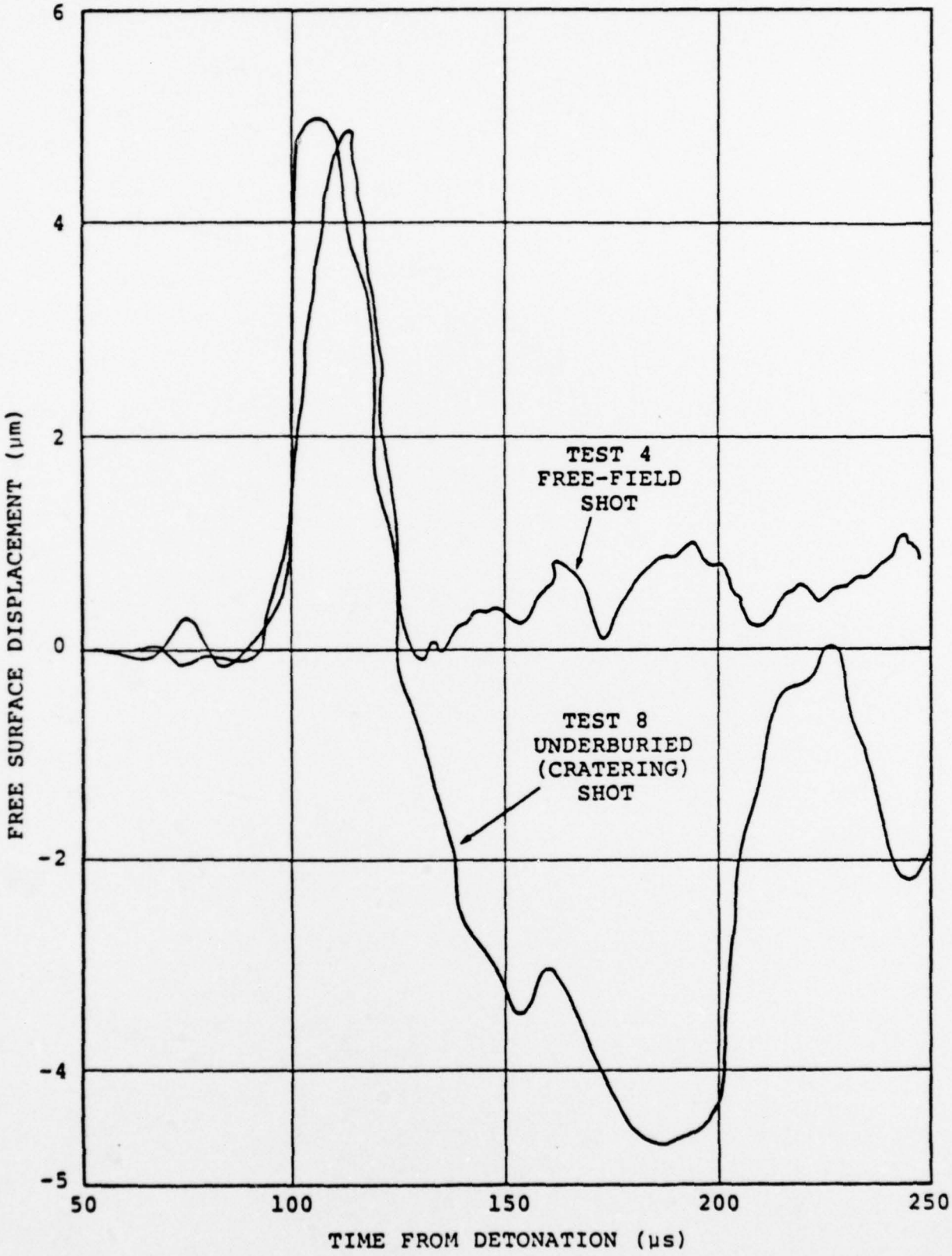

Figure 3.3. The displacement-time histories are compared from the free-field Experiment 4 and the cratering Experiment 8.

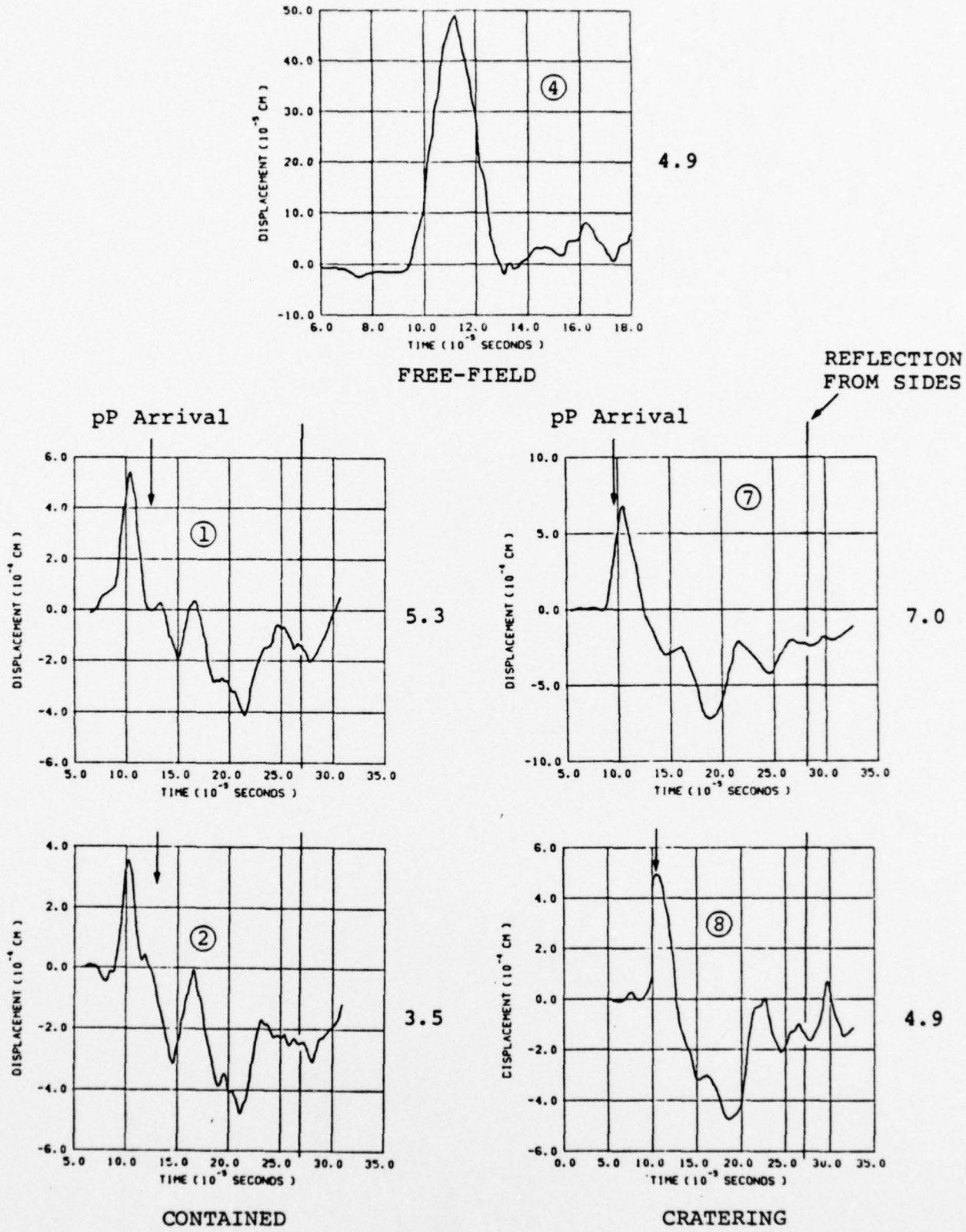

Figure 3.4. The displacement-time histories are plotted for the five experiments to be further analyzed. The test identifier from Table 3.1 is noted on each plot. At the right are the amplitudes of the peak displacement in microns. On the plots for the contained and cratering experiments we show the expected arrival times (from elastic theory) of the free surface pP phase and the unwanted reflections from the sides of the cylinder.

For the experiments that cratered the energy in the pP pulse is expected to be lost in the cratering process. Indeed, the cratering records differ from those from the contained explosion by the absence of an apparent pP pulse. But they do have a large negative pulse that seems to have very much the same character as that on the contained records. The lag time between this pulse and the direct wave appears to be proportional to the depth.

What is the origin of the large negative phase? It seems to be due to the relaxation of the locked-in stresses around the cavity, the stresses that form the "containment membrane," when the presence of the free surface is sensed. In essence the cavity and environs relax toward the free surface. This phenomenon was discussed by Dr. J. Trulio of Applied Theory, Inc. (ATI), at several ARPA sponsored meetings in 1976-1977. Dr. Trulio noticed a similar large negative pulse in full-scale nuclear cratering calculations carried out at ATI. There is some feeling that gravity, which is present in his calculations, has some role in generating this phase. However, there are no gravitional effects in our small-scale experiments.

In the remainder of this section we will attempt to determine the potential significance of the experimental results for the teleseismic body wave signatures of underground nuclear explosions.

3.3 AN EQUIVALENT ELASTIC SOURCE

For the free-field experiments it is easy to determine an equivalent elastic source suitable for propagating the ground motion to any desired distance. The ground motion is

recorded on a surface normal to the spherical wave from the charge. The free surface coefficient is then merely two. Dividing by two, the displacment-time history is the same as the R displacement for a spherically symmetric explosion in a whole-space. The natural form for the equivalent elastic source is then the reduced displacment potential, Ψ, which is related to the displacement, u, by

$$u(R,t) = \frac{\Psi(\tau)}{R^2} + \frac{\dot{\Psi}(\tau)}{R\, v_p} \quad , \tag{3.1}$$

$$\tau = t - R/v_p \quad .$$

With R the distance between the charge and the free surface, this equation can be inverted to solve for $\Psi(\tau)$ from the recorded displacement.

For the contained and cratering experiments, Equation (3.1) cannot be applied rigorously. It is true that the recorded ground motion still differs from that in a continuous medium by a constant factor, two. However, the wave is no longer a simple spherical wave from a point source but is composed of a spherical wave from the charge, another nearly spherical wave (pP) from the free surface and the large negative pulse which may or may not be spherical in its decay.

Keeping in mind the limitations pointed out in the previous paragraph, we construct an approximate equivalent elastic source by applying Equation (3.1) to the cratering and contained explosion data in the same way we used it for the free-field data. The geometry is shown in Figure 3.5.

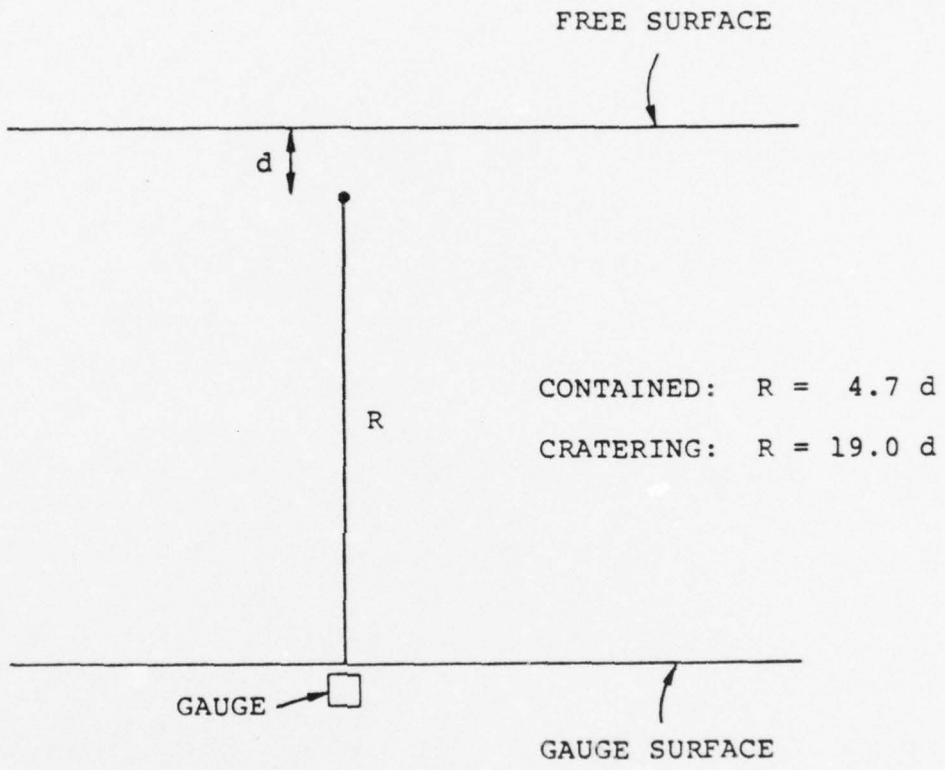

Figure 3.5. The geometry is shown schematically for the contained and cratering experiments.

The approximate RDP representation used here should suffice for at least a rough estimate of the effect of the free surface on the far-field body waves compared to the theoretical effect predicted by elastic theory. Among the justifications for using this approximation is the fact that $R >> d$ as indicated in Figure 3.5. Also, the important takeoff angles for far-field body waves are near the downward vertical.

Applying Equation (3.1) to the data in Figure 3.4, we compute a $\dot{\Psi}(\tau)$ for each of the five experiments. The far-field ($R >> 1$) displacement is proportional to $\dot{\Psi}(\tau)$. This quantity is plotted in Figure 3.6. Comparing Figures 3.4 and 3.6, we see that our data are not much affected by the near-field term in Equation (3.1).

For convenience in propagating the reduced displacement potential to the far-field, we need to obtain the Fourier transform of $\dot{\Psi}(\tau)$. For this we need a $\dot{\Psi}(\tau)$ that vanishes at long time (equivalent to a source displacement-time history that achieves a constant static displacement). The late time data in Figure 3.6 are contaminated by reflections from the sides of the cylinder as indicated. With this in mind, the first step in the Fourier transformation is to damp the $\Psi(\tau)$ to zero at times just before those when the unwanted reflections arrive. The results are shown in Figure 3.7.

The $\dot{\Psi}(\tau)$ of Figure 3.7 are Fourier transformed and the resulting amplitude spectra are shown in Figure 3.8. A natural question to ask about these spectra is, how much are they influenced by the damping to zero which is done somewhat arbitrarily? The answer is, not very much, as is demonstrated in Figure 3.9. The amplitude spectra in this figure were obtained by Fourier transforming the original $\dot{\Psi}(\tau)$ from Figure 3.6. In our numerical Fourier transformation, the actual function transformed is $\phi(t)$ where

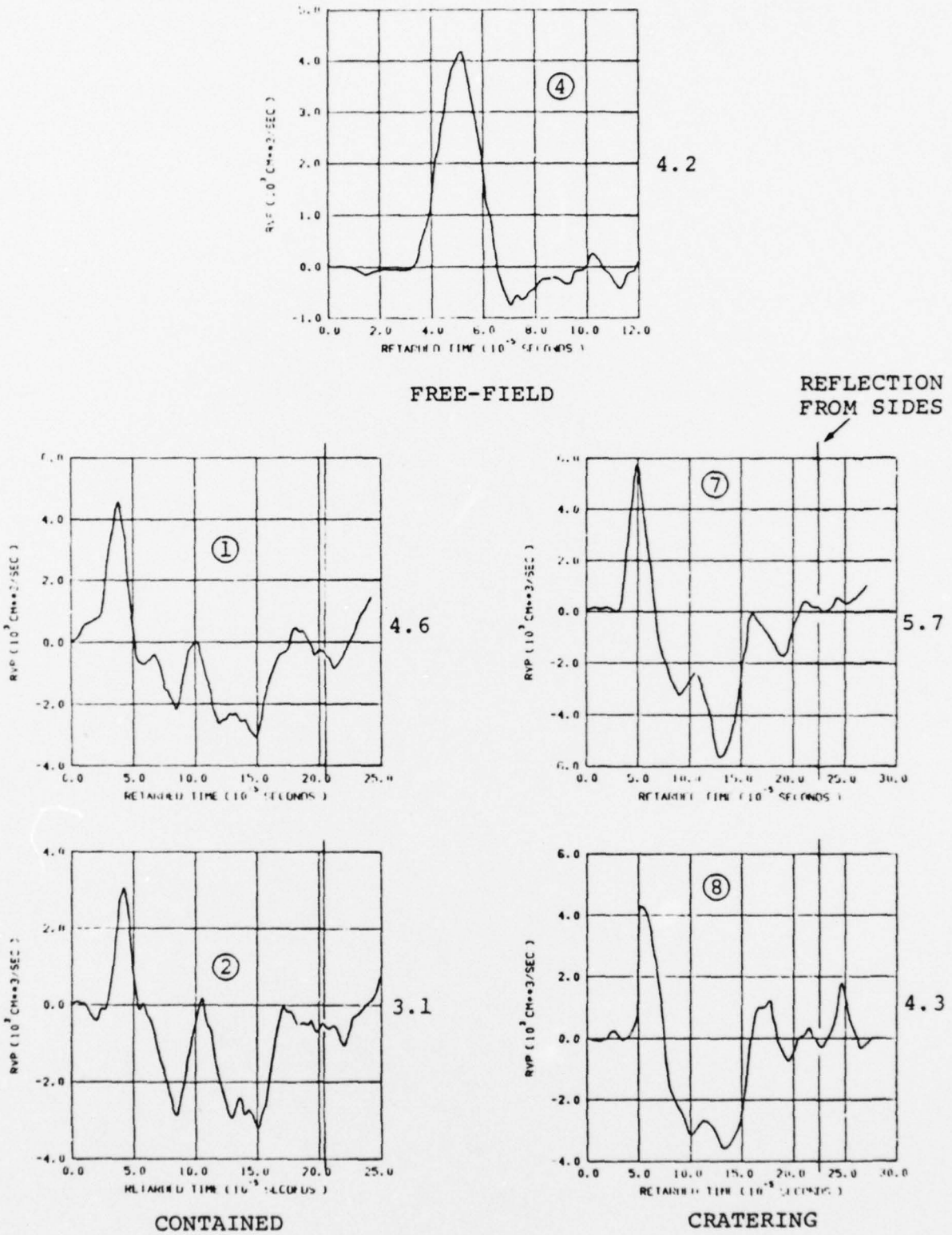

Figure 3.6. The far-field displacement $[\dot{\Psi}(\tau)]$ is plotted for the five experiments being analyzed. The peak values are indicated at the right of each plot and the theoretical arrival time for reflections from the sides of the cylinder is indicated.

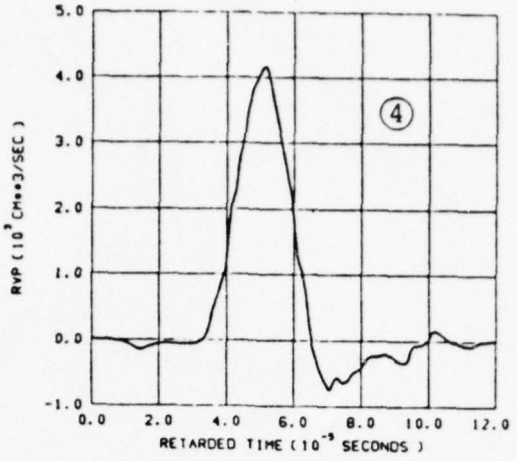

FREE-FIELD

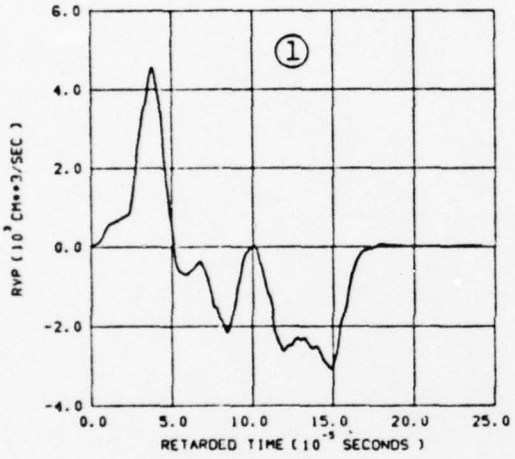

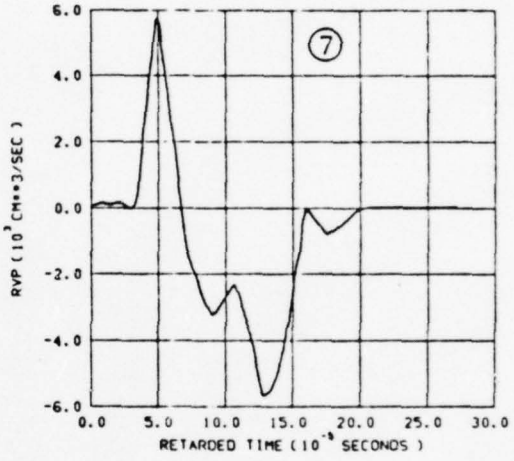

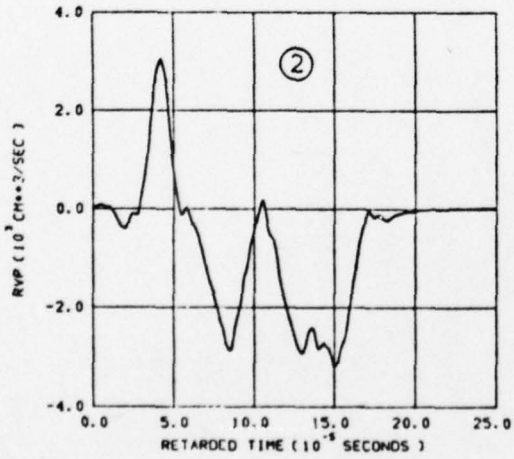

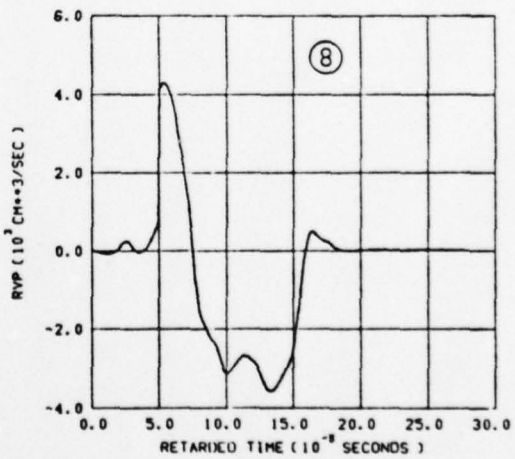

CONTAINED

CRATERING

Figure 3.7. The $\dot{\Psi}(\tau)$ are plotted after damping the signal to zero near the arrival time for reflections from the sides of the cylinder.

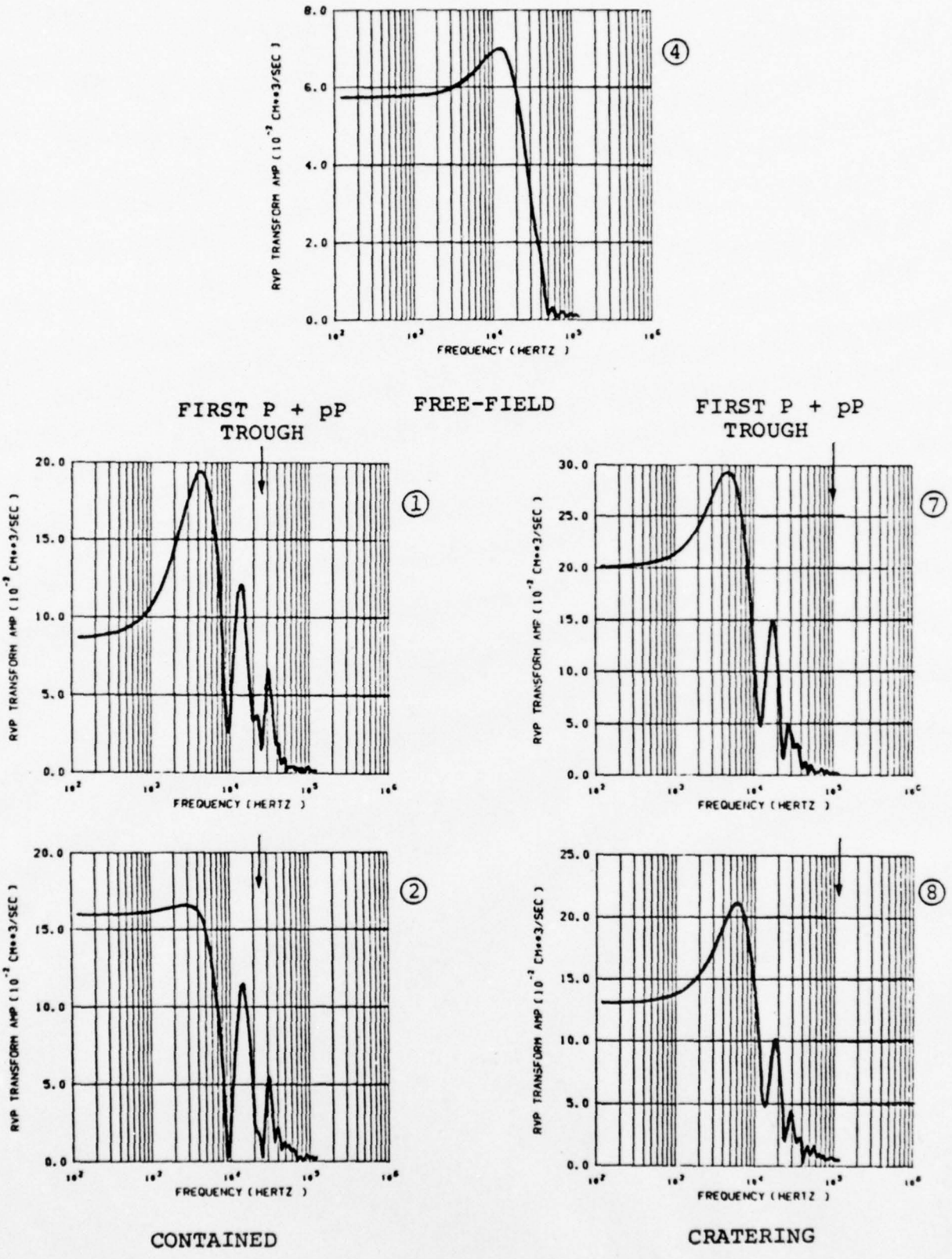

Figure 3.8. The amplitude spectra, $|\hat{\Psi}(\omega)|$, resulting from Fourier transformation of the signals of Figure 3.7 are shown.

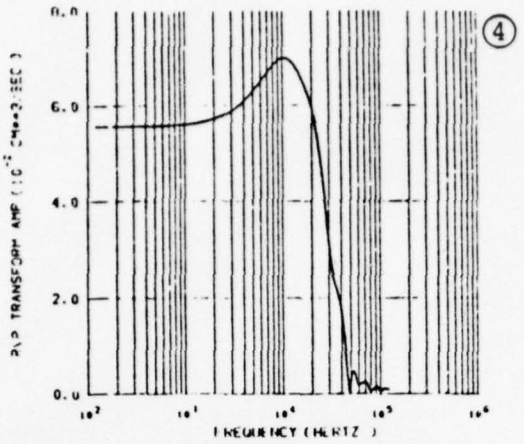

FREE-FIELD

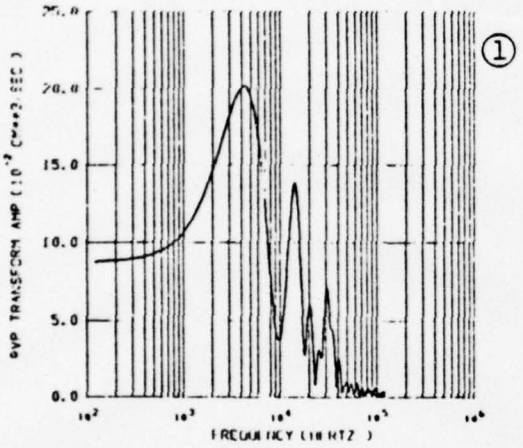

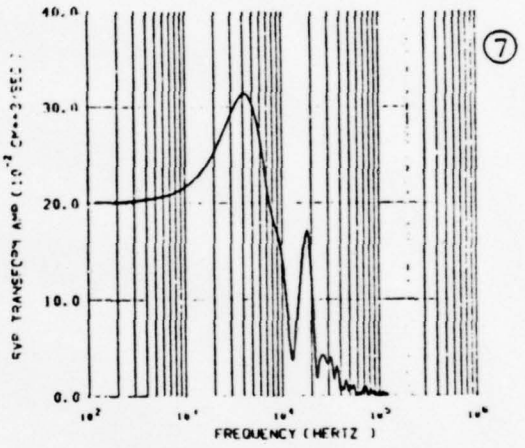

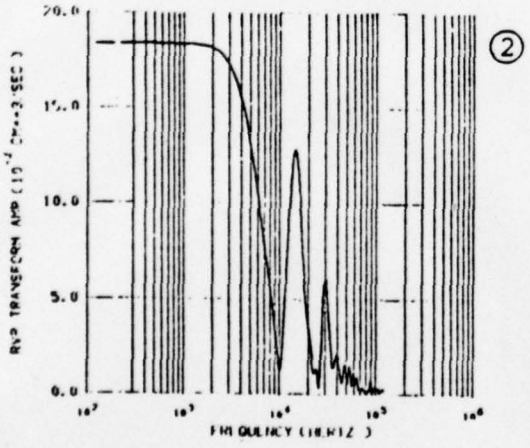

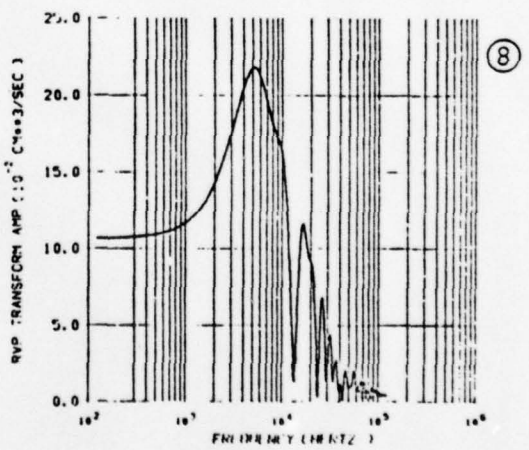

CONTAINED

CRATERING

Figure 3.9. The amplitude spectra, $|\hat{\Psi}(\omega)|$, resulting from Fourier transforming the undamped $\Psi(\tau)$ from Figure 3.6 are shown.

$$\phi(t) = \begin{cases} \dot{\Psi}(t) \ , \ 0 \leq t \leq \tau_{max} \ , \\ 0 \ , \ \tau_{max} < t \ , \end{cases} \tag{3.2}$$

where τ_{max} is the time of the last nonzero value of $\dot{\Psi}(\tau)$. In transforming the $\dot{\Psi}(\tau)$ from Figure 3.4 we are then transforming functions that are zero beyond the points plotted. The differences between the amplitude spectra in Figures 3.8 and 3.9 are almost entirely at the long period end and even there are not very great.

The spectra for the contained and cratering experiments differ from that for the free-field experiment by the absence of spectral scalloping in the latter. This scalloping is due to interference between the direct P wave and the negative phases associated with the presence of the free surface. The expected position (from elastic theory) of the P+pP spectral trough is indicated on the plots. Clearly, the later arriving, nonelastic negative pulse is dominant in shaping these spectra.

3.4 COMPARISON OF EXPERIMENTAL SOURCE SPECTRA TO THOSE FROM UNDERGROUND NUCLEAR EXPLOSIONS

The source spectra obtained from the experimental data were plotted in Figure 3.8. How do these compare to those from underground nuclear explosions? In Figure 3.10 are shown typical theoretical source spectra for an underground nuclear explosion. One of these is for a spherically symmetric source in a whole space and, therefore, is free-field. Except for the great difference in scale, this spectrum looks very much like the experimental free-field spectrum in Figure 3.8.

The second nuclear source spectrum in Figure 3.10 was constructed by lagging the free-field spectrum by 0.55 seconds and summing it to itself. The resulting spectrum

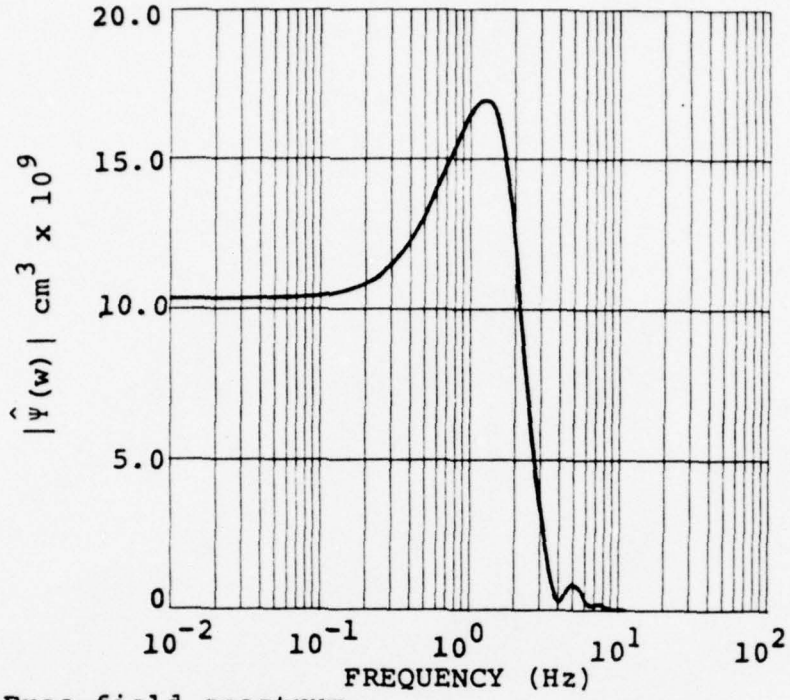

(a) Free-field spectrum

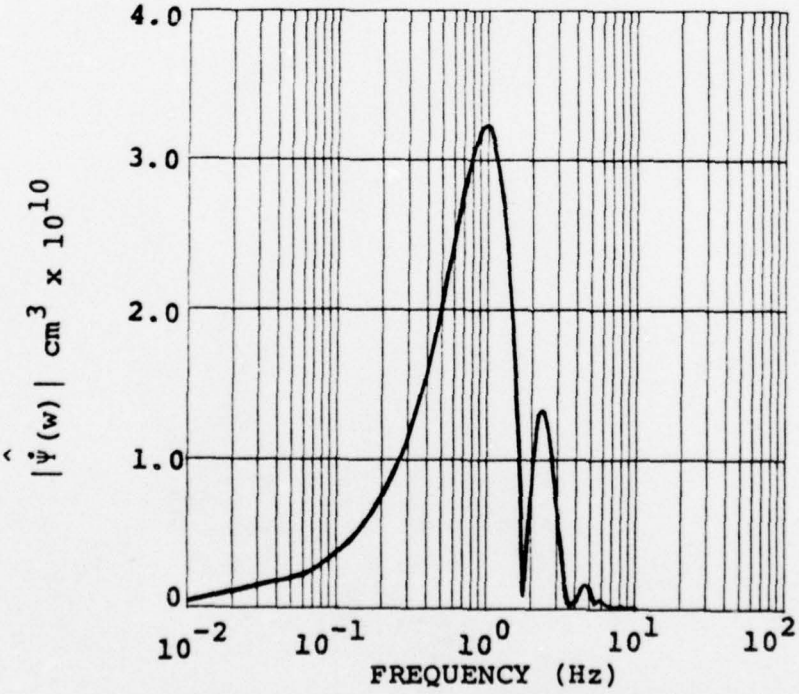

(b) The spectrum of (a) is summed to itself after lagging by 0.55 seconds.

Figure 3.10. Theoretical source spectra are shown for a contained nuclear explosion in Yucca Flat saturated tuff (source 133 from Bache et al., 1975). The yield is 20 Kt.

is scalloped, with holes occurring at frequencies that are multiples of the inverse of the lag time (0, 1.8, 3.6 Hz, etc.). If we compare this spectrum to those from the contained and cratering experiments in Figure 3.8, we see that they have a similar form. However, keep in mind that the spectral holes in the experimental spectra are mainly due to the nonelastic negative pulse rather than the pP phase.

Comparing the theoretical nuclear explosion spectra and those from the experiments, it appears that the only substantial difference is in the time scale. For the nuclear explosion the peak in the free-field spectrum occurs at about 1.3 Hz. The comparable value for the experiments is 1.3×10^4 Hz. Thus, the time scales differ by about 10^4. The ratio of the peak amplitudes is about 0.24×10^{12}.

If we are to determine the potential effects of a free surface phase like that seen in the experiments on the teleseismic signatures of nuclear explosions, the experimental results must be scaled to a comparable frequency range. A natural way to do this is to cube-root scale the experimental results by a yield ratio of 10^{12}. The experimental spectra would then have about the same amplitude and frequency content as the nuclear explosion spectra. As far as the elastic behavior of the source is concerned, in particular the P-pP lag time, this scaling seems quite reasonable.

In subsequent subsections, much of our attention will be focused on the large nonlinear negative pulse. The degree to which the waveform (frequency content) of this pulse can be cube-root scaled is certainly open to question. The time delay between the arrival of the direct wave and this pulse seems to be depth controlled and perhaps more closely follows a cube-root scaling law. In any event, cube-root scaling seems to be the best we can do and should give instructive results.

In Figure 3.11 we show cube-root scaled spectra for the free-field experiment and one of the contained-charge experiments. The scaling is by four different yield scaling factors, denoted by W. These factors are summarized in Table 3.2 together with other data about the scaling. The "nuclear explosion equivalent yield" is the yield at which the source of Figure 3.10 has about the same frequency content. The scaled depth of burial and P-pP lag are calculated by cube-root scaling the actual depth (6.5 cm, see Table 3.1) and theoretical P-pP lag time of Experiment 1. These numbers provide some verification of our scaling since the depths in the table are only a factor of two greater than standard burial depths for the equivalent yields in the table. This means that the dominant period of the P waves for our scaled experiments will bear about the same relation to the P-pP lag time as it does in a contained nuclear explosion.

3.5 IMPLICATIONS OF THE EXPERIMENTAL RESULTS FOR TELESEISMIC BODY WAVES

Having the source in the form of an equivalent elastic source, in this case a reduced displacement potential, we can compute theoretical seismograms employing the same techniques used in numerous past S^3 reports (e.g., Bache, 1976; Bache and Harkrider, 1976; Bache, et al., 1975). For these calculations we use a standard path model (C2 from Anderson and Hart, 1976) and $t^* = 0.7$. Two kinds of calculations were done. In the first kind the (scaled) free-field source was emplaced at the appropriate scaled burial depth from Table 3.2. In this case the dominant phases on the seismogram are P and pP with the time lag being about that in Table 3.2. There are also some small reverberations caused by the earth model, particularly the crust in the receiver vicinity. For the contained and cratering calculations, the near-source free surface effects are already

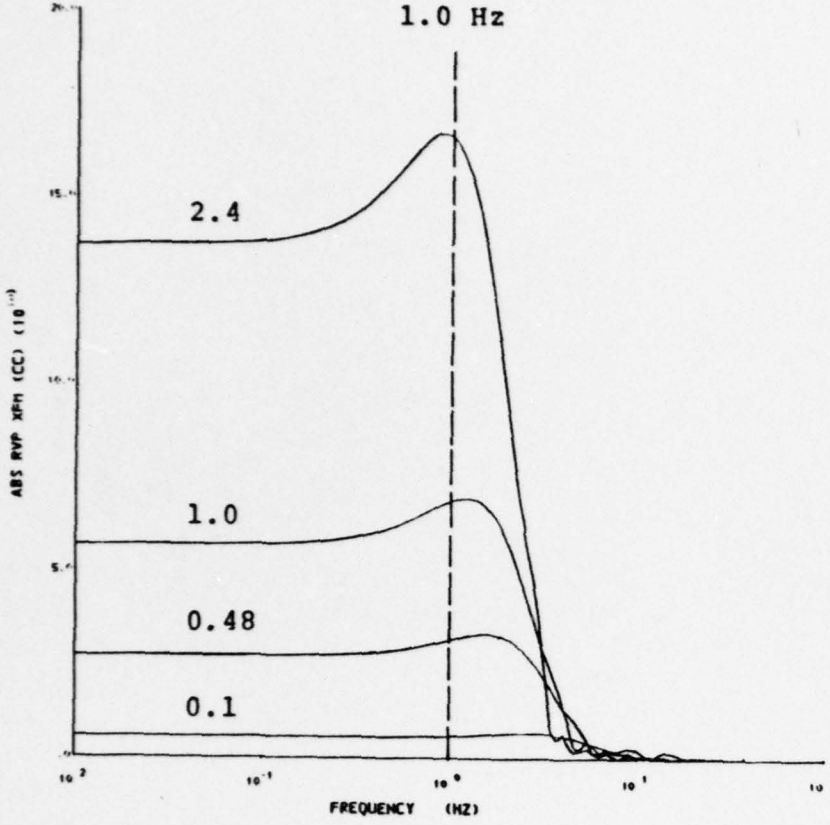

(a) Scaled $|\hat{\Psi}(\omega)|$ from Test 4.

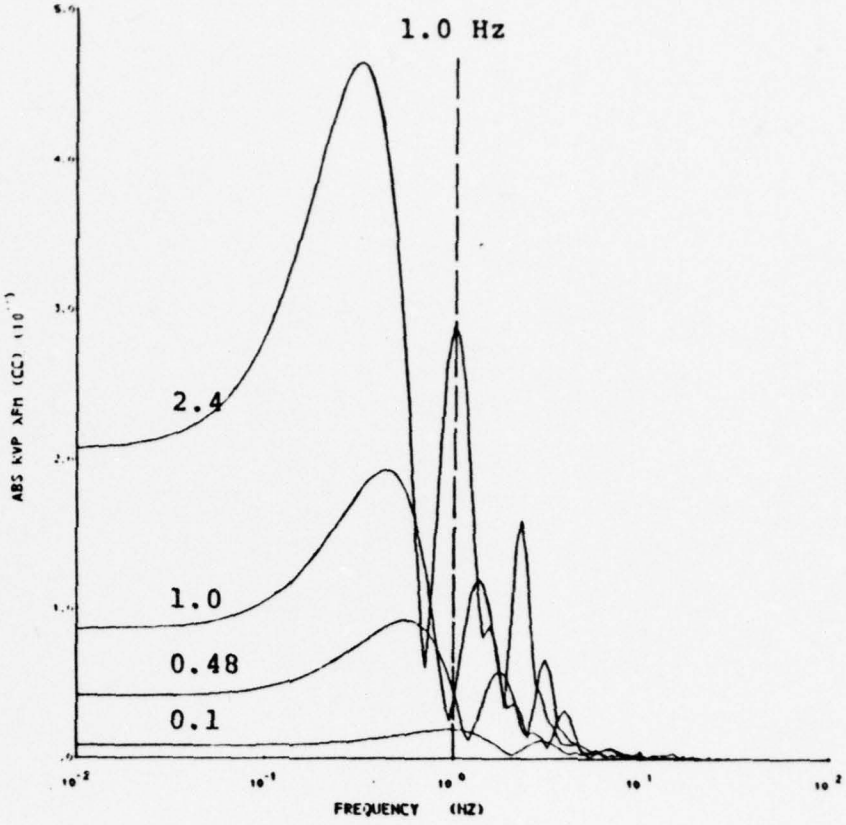

(b) Scaled $|\hat{\Psi}(\omega)|$ from Test 1.

Figure 3.11. The spectral amplitudes from Experiments 1 and 4 are plotted after scaling by four scaling factors, W. The values indicated on the plots are to be multipled by 10^{12} to obtain W.

TABLE 3.2

PARAMETERS FOR THE SCALING OF CONTAINED EXPERIMENT NO. 1

Yield Scale Factor W	Nuclear Explosion Equivalent Yield	Scaled Depth of Burial (meters)	Scaled P-pP Lag (sec)
2.4×10^{12}	48.0 Kt	870	0.52
1.0×10^{12}	20.0 Kt	650	0.39
0.48×10^{12}	9.6 Kt	509	0.30
0.1×10^{12}	2.0 Kt	302	0.18

included in the source representation. Therefore, for theoretical seismograms for these sources the free surface in the source region is not included in the calculation.

The theoretical seismograms for the five experiments (one free-field, two contained and two cratering) scaled by four different factors are shown in Figure 3.12. First, with respect to the waveforms we point out the following:

- The seismograms for the two contained and two cratering experiments are nearly the same.
- The free-field experiments demonstrate the theoretical effect of the elastic pP. Even at the greatest lag time (0.50 seconds) the waveform shows no interference pattern.
- The large nonlinear negative pulse arrives much later than the pP, but at times proportional to the burial depth (compare events at the same scaled depth, independent of W).
- At the larger scaled depths the nonlinear negative pulse causes the seismograms to be markedly different than they would be if only the elastic P and pP were present.

What is the effect of the free surface phases on m_b? To answer these questions we computed m_b for each of the seismograms by measuring the amplitude and period of the "c" phase or first-trough to second-peak. The period of this phase is indicated on each seismogram in Figure 3.12. The m_b data are summarized in Table 3.3.

For directly comparing the amplitudes of the seismograms in Figure 3.12 we have a problem in that the coupling into seismic waves was not identical for all sources. To see this

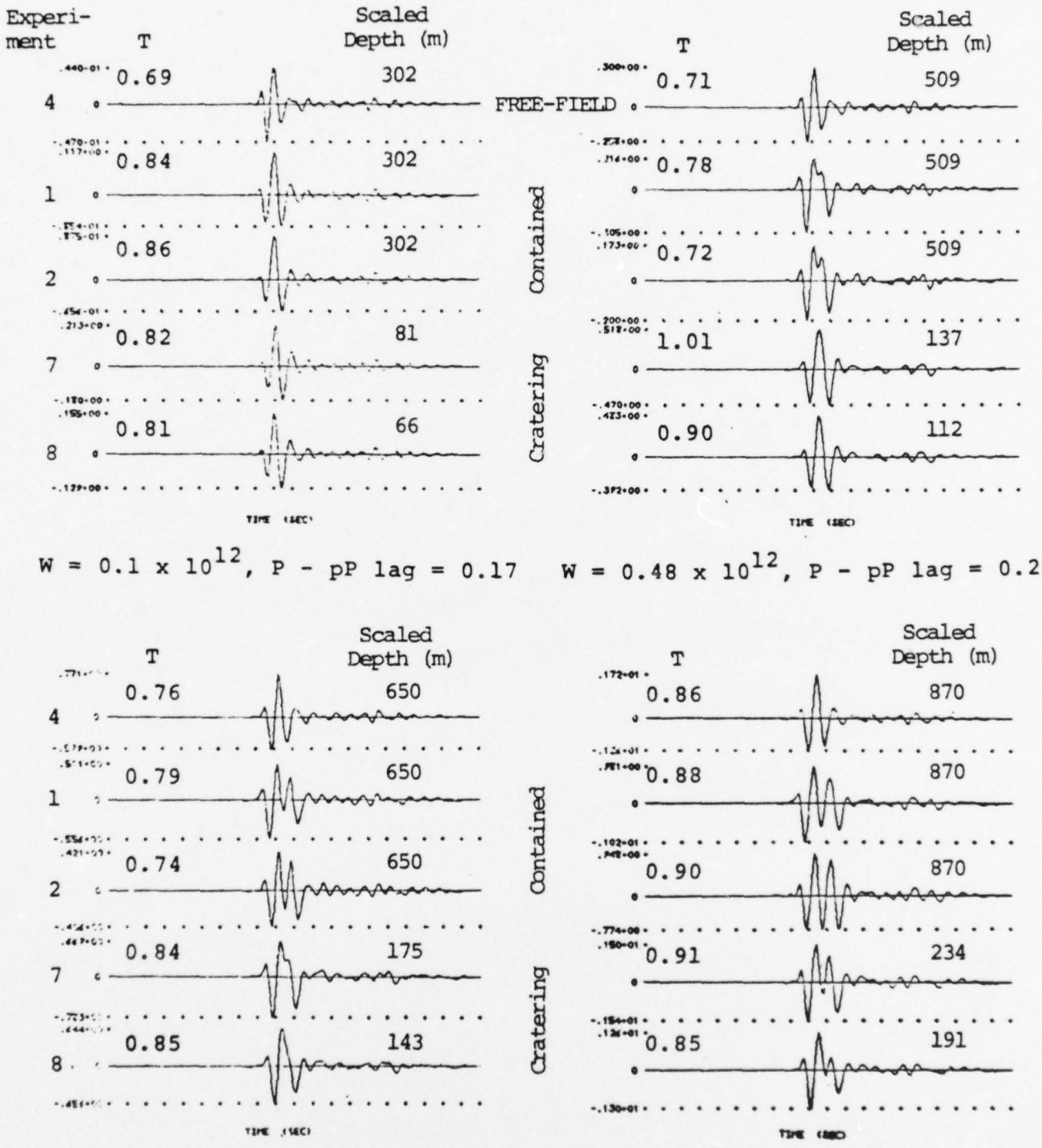

Figure 3.12. The theoretical seismograms are shown for the five experimental sources scaled by four yield factors.

TABLE 3.3

MAGNITUDE DATA FOR THE SEISMOGRAMS OF FIGURE 3.12

Experiment	Normalizing* Correction	m_b W 0.1×10^{12}	Normalized* W 0.48×10^{12}	m_b W 1.0×10^{12}	W 2.4×10^{12}
4 (Free-field)	0	3.77	4.58	5.01	5.41
1 (Contained)	-0.03	4.19	4.55	4.87	5.22
2 (Contained)	+0.15	4.26	4.55	4.92	5.34
7 (Cratering)	-0.17	4.32	4.82	4.89	5.23
8 (Cratering)	-0.02	4.32	4.85	5.01	5.31

*See text

we go back to the displacement time histories in Figure 3.4. The peak displacements are indicated in the figure and vary from 7.0 to 3.5, a factor of two. The peak displacement is probably as good a measure of the coupling as we have, so we normalized the seismogram amplitudes by the ratio of the peak displacements to that for Test 4, the free-field test. The logarithm of this ratio is shown in Table 3.3 as the "Normalizing Correction." Thus, for example, the "raw" m_b values for the Experiment 7 seismograms shown in Figure 3.12 are 0.17 m_b units higher than the normalized values shown in Table 3.3.

There are two independent checks on the validity of the normalization procedure described in the previous paragraph. First, the results are essentially the same if, instead of normalizing the peak displacement, we normalize the peaks of the $\dot{\Psi}(\tau)$ in Figure 3.6. Second, the normalization brings the m_b values for the two contained and two cratering experiments into much closer agreement.

The most important result of this study is presented in Figure 3.13 where the m_b values from Table 3.3 are plotted versus the yield factor. These are, in essense, m_b-yield data and we fit linear curves to m_b versus the logarithm of the yield factor. Recognizing that several approximations were made in obtaining the equivalent elastic source from the experimental data and in cube-root scaling these sources, the data in Figure 3.13 give a clear indication of the kind of effects to be expected if a large nonlinear negative pulse like that in the experimental data is also present in underground nuclear explosions. The slope of the magnitude-lag yield curve is substantially reduced.

The elastic calculations using the free-field source at burial depths proportional to yield give a slope of 1.2. Theoretical studies in which the source cube-root scales with yield and is independent of depth always show large slopes like

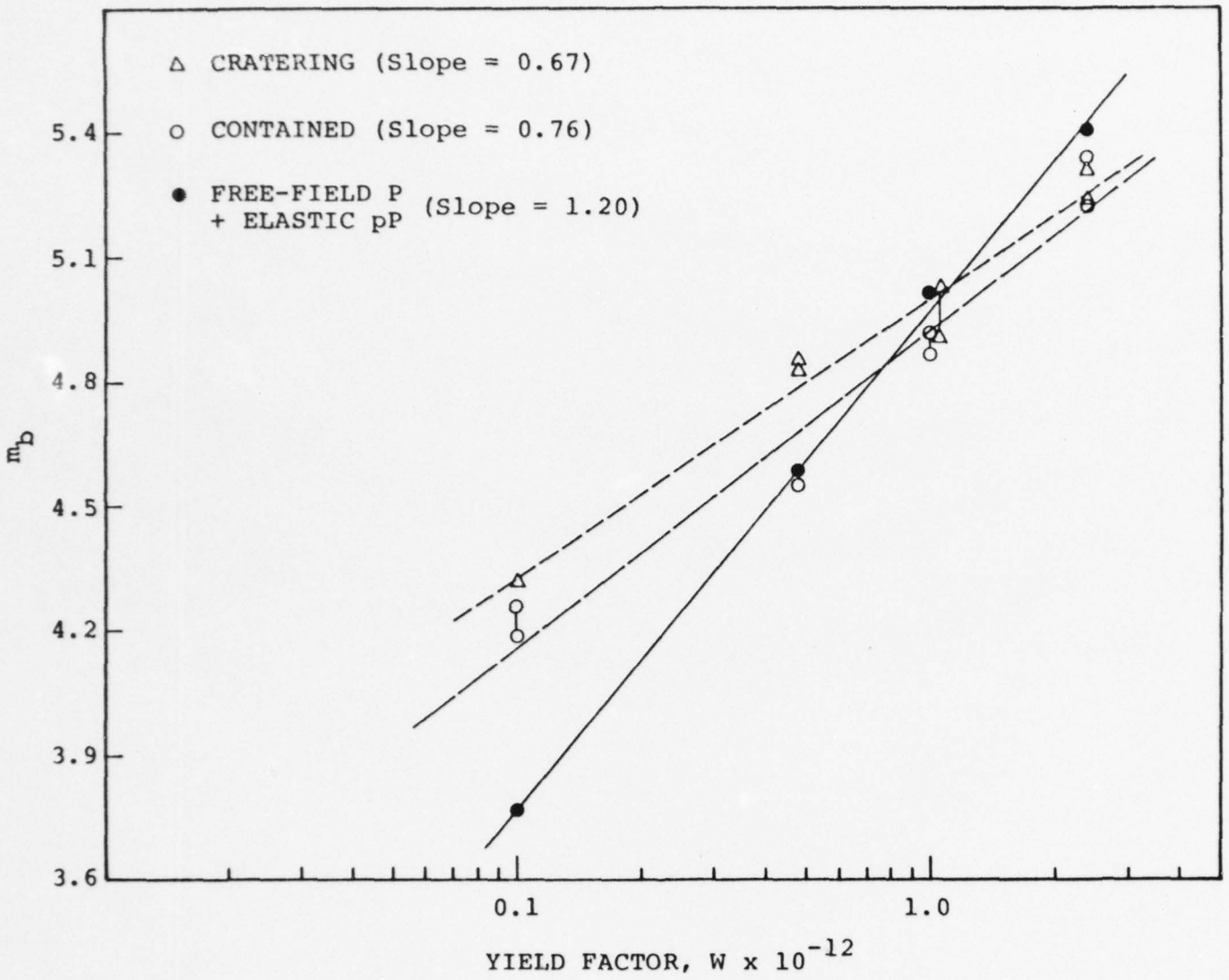

Figure 3.13. The m_b data from Table 3.3 are plotted and fit, in the least squares sense, by a linear relationship to log W.

this (e.g., Bache, Cherry and Mason, 1976). Theoretical slopes close to unity are usually obtained by supposing, with some justification, that the source coupling is in some way inversely proportional to depth (e.g., Bache, Cherry and Mason, 1976).

The differences between the contained and cratering m_b-log yield curves are fairly small and may not be meaningful in view of the approximations made. Still, it is interesting to note that the contained experiments, which do have a noticeable pP contribution (Figure 3.4), result in a larger slope.

The most important conclusion one can draw from this study is that if nuclear explosions have a large late-time negative pulse analogous to that in the experiments, the m_b values are influenced. In fact, this pulse is expected to cause a reduction in the m_b-log yield slope and, if present, may explain why the observed slopes are less than predicted by theoretical models which treat the free surface effect as elastic.

REFERENCES

Alewine, R. W., (1974), "Application of Linear Inversion Theory Toward the Estimation of Seismic Source Parameters," Ph.D. Thesis, California Institute of Technology.

Alexander, S. S., (1963), "Crustal Structure in the Western United States from Multi-Mode Surface Wave Dispersion," Ph.D. Thesis, California Institute of Technology.

Bache, T. C., J. T. Cherry, N. Rimer, J. M. Savino, T. R. Blake, T. G. Barker and D. G. Lambert, (1975), "An Explanation of the Relative Amplitude Generated by Explosions in Different Test Areas at the Nevada Test Site," Systems, Science and Software Final Contract Report, DNA 3958F.

Bache, T. C. (1976), "The Effect of Tectonic Stress Release on Explosion P-Wave Signatures," BSSA, 66, 1441-1457.

Bache, T. C., J. T. Cherry, D. G. Lambert, J. F. Masso and J. M. Savino (1976), "A Deterministic Methodology for Discriminating Between Earthquakes and Underground Nuclear Explosions," Systems, Science and Software Final Technical Report submitted to ARPA, SSS-R-76-2925, July 1976.

Bache, T. C., J. T. Cherry and B. F. Mason (1976), "The Dependence of Body Wave Magnitude on Yield for Underground Explosions in Salt," Systems, Science and Software Topical Report, SSS-R-77-3057, November 1976.

Bache, T. C. and D. G. Harkrider (1976), "The Body Waves Due to a General Seismic Source in a Layered Earth Model: 1. Formulation of the Theory," BSSA, 66, 1805-1819.

Bache, T. C., J. M. Savino, M. Baker and P. L. Coleman (1977), "Seismic Studies for Improved Yield Determination," Systems, Science and Software Quarterly Technical Report submitted to AFTAC/VSC, SSS-R-77-3108, January 1977.

Backus, G. and F. Gilbert (1970), "Uniqueness in the Inversion of Inaccurate Gross Earth Data," Phil. Trans. Roy. Soc. London, Ser. A 266, 123-192.

Barker, T. G., M. Baker, P. L. Coleman and D. G. Lambert (1977), "Seismic Studies for Improved Yield Determination," Systems, Science and Software Quarterly Technical Report SSS-R-77-3191, April 1977.

Diment, W. H., S. W. Stewart, and J. C. Roller (1961), "Crustal Structure from the Nevada Test Site to Kingman, Arizona, from Seismic and Gravity Observations," J. Geophys. Res., 66, 201-214.

Harkrider, D. G., (1964), "Surface Waves in Multilayered Media I. Rayleigh and Love Waves from Buried Sources in a Multilayered Elastic Half-Space," BSSA, 54, 627-679.

Harkrider, D. G., (1970), "Surface Waves in Multilayered Media II. Higher Mode Spectra and Spectral Ratios from Point Sources in Plane-Layered Earth Models," BSSA, 60, 1937-1987.

Harkrider, D. G. and C. B. Archambeau (1977), "Theoretical Rayleigh and Love Waves from an Explosion in Prestressed Source Regions," (to be submitted for publication).

Haskell, N. A. (1967), " Analytic Approximation for the Elastic Radiation from a Contained Underground Explosion," J. Geophys. Res., 72, 2583-2587.

Johnson, L. E. and F. Gilbert (1972), "Inversion and Inference for Teleseismic Ray Data," Methods in Computational Physics, 12, B. A. Bolt (Editor), 231-266.

Jordan, T. H. (1973), "Estimation of the Radial Variation of Seismic Velocities and Density in the Earth," Ph.D. Thesis, California Institute of Technology.

Keller, G. R., R. B. Smith, L. W. Braile, R. Heaney and D. H. Shurbet (1976), "Upper Crustal Structure of the Eastern Basin and Range, Northern Colorado Plateau and Middle Rocky Mountains from Rayleigh-Wave Dispersion," Bull. Seism. Soc. Am., 66, 869-876.

Langston, C. A. and D. V. Helmberger (1974), "Interpretation of Body and Rayleigh Waves from NTS to Tucson," Bull. Seism. Soc. Am., 64, 1919-1929.

McGarr, A., and L. E. Alsop, (1967), "Transmission and Reflection of Rayleigh Waves at Vertical Boundaries," J. Geophys. Res., 72, 2169-2180.

McGarr, A., (1969), "Amplitude Variations of Rayleigh Waves - Propagation Across a Continental Margin," BSSA, 59, 1281-1305.

Mitchell, B. J. (1975), "Regional Rayleigh Wave Attenuation in North America," J. Geophys. Res., 80, 4904-4916.

Prodehl, C. (1970), "Seismic Refraction Study of Crustal Structure in the Western United States," Geol. Soc. of Amer. Bull., 81, 2629-2646.

Rodi, W. L., P. Glover, T. M. C. Li, and S. S. Alexander (1975), "A Fast, Accurate Method for Computing Group-Velocity Partial Derivatives for Rayleigh and Love Modes," Bull. Seism. Soc. Am., 65, 1105-1114.

Springer, D. L., and R. L. Kinnaman (1971), "Seismic Source Summary for U. S. Underground Nuclear Explosions," BSSA, 61, 1073-1098.

Takeuchi, H., J. Dorman and M. Saito (1964), "Partial Derivatives of Surface Wave Phase Velocity with Respect to Physical Parameter Changes Within the Earth," J. Geophys. Res., 69, 3429-3441.

Toppozada, T. R. and A. R. Sanford (1976), "Crustal Structure in Central New Mexico Interpreted from the Gasbuggy Explosion," Bull. Seism. Soc. Am., 66, 877-886.

Warren, D. H. (1969), "A Seismic-Refraction Survey of Crustal Structure in Central Arizona," Geol. Soc. of Amer. Bull., 80, 257-282.

Wiggins, R. A. (1972), "The General Linear Inverse Problem: Implication of Surface Waves and Free Oscillations for Earth Structure," Rev. Geophys., 10, 251-285.

APPENDIX A

ABSTRACTS OF TECHNICAL REPORTS SUBMITTED TO AFTAC/VSC, MAY 1975 - OCTOBER 1977

4.1 QUARTERLY REPORTS

● August 8, 1975, "Improved Yield Determination a vent Identification Research," J. T. Cherry, N. Rimer, J. M avino and W. O. Wray, SSS-R-75-2696.

A one-dimensional parameter study which ide ies the dependence of teleseismic magnitude on near source rial properties was carried out. The major results o terial parameter sensitivity study may be summarized as ll s: (1) increasing the air-filled porosity greatly re es seismic coupling; (2) if any parameter describing the yield surface is varied such that the material strength is reduced, seismic coupling may be substantially enhanced; (3) seismic coupling is relatively insensitive to water content; a slight decoupling is observed with increasing water content; (4) increasing the overburden pressure substantially reduces seismic coupling.

The near field coupling and the equivalent source were computed for the recent underground explosion, MAST, at Pahute Mesa. The next step is to generate synthetic seismograms for this event at recently specified receiver locations. The enhanced computational capabilities for treating realistic earth structures will be exercised in this experiment.

● November 17, 1975, "Improved Yield Determination and Event Identification Research," J. M. Savino, T. C. Bache, T. G. Barker, J. T. Cherry and W. O. Wray, SSS-R-76-2788.

Teleseismic ground motion predictions for the recent Pahute Mesa explosion MAST, were quite successful in terms of both amplitude and waveform matching. The predicted short-period

body wave amplitudes were within 30 to 50 percent of the observed amplitudes at most of the SDCS stations. In addition, the general character of the first few seconds of the P-wave trains at the various SDCS stations were matched in reasonable detail.

A tension failure model that describes the development of a region of enhanced tension failure (cracking) produced during stress release behind the interacting shock fronts from closely spaced explosions was developed. Calculations for a multiple explosion scenario (three closely spaced explosions detonated simultaneously) were carried out into the elastic region using the two-dimensional CRAM code with the new material failure model included.

- February 1976, "Improved Yield Determination and Event Identification Research," J. M. Savino, SSS-R-76-2870.

Comparison of computed and observed short and long period seismograms for the Pahute Mesa explosion, MAST, were made with respect to amplitude, waveform and travel times. Travel times were closely matched as were the waveforms for surface waves recorded at the SDCS stations. For body waves a number of the SDCS stations are within the triplication range and the waveform match was far from ideal. Still, amplitudes for both body and surface waves were matched to within 50 percent and were much closer in most cases.

- May 1976, "Explosion Source Modeling, Seismic Waveform Prediction and Yield Verification Research," T. C. Bache, T. G. Barker, J. T. Cherry, N. Rimer and J. M. Savino, SSS-R-76-2924.

The theoretically computed and observed amplitudes of both b and d (maximum) body wave phases for KASSERI agree to well within a factor of two at all of the five SDCS stations. Minor adjustments of the upper mantle model could improve the agreement at all the SDCS sites.

Computations of the effect of material strength on teleseimic body wave amplitudes indicate that the amplitude of the b phase increases with decreasing strength; the rate of increase being more rapid at lower levels of material strength. An additional effect is that the apparent period of the b phase increases rapidly with decreasing strength due to a shift in the corner frequency of the source spectrum.

Further verification of the explosion source modeling code, SKIPPER, was achieved by comparison of free field ground motion calculations and observations for the PILEDRIVER and GASBUGGY explosions. In the case of PILEDRIVER, the exercise of a recently developed elastic wave propagation code verified that the observed PILEDRIVER RDP was not affected by reflected waves from the free surface or from layer interfaces in the source region.

Excellent free field ground motion measurements and material properties data are available for the GASBUGGY explosion. The computed RDP, employing these data, agrees quite well with the measured RDP, increasing our confidence in the constitutive modeling of the explosion source and ultimately the teleseismic ground motion predictions based on these source calculations.

- August 1976, "Explosion Yield Verification, Multiple Explosion Scenarios and Three-Dimensional Seismic Modeling Research," D. G. Lambert, C. F. Petersen and J. M. Savino, SSS-R-76-2993.

A procedure for directly inverting teleseismic ground motion data in order to obtain estimates of explosion yields was developed. The particular inversion scheme employs a deterministic modeling capability which predicts the telesismic

ground motion from a nuclear explosion. This procedure supplements expected data exchange packages that provide information on the near explosion source environment.

Experiments involving computer simulation and decomposition of multiple explosion scenarios were recently initiated. Application of narrow-band filtering to synthesized multiple event seismograms has yielded accurate determinations of the relative amplitudes and time separations between individual explosions in the multiple explosion event examined.

Preparations are nearing completion for a series of three-dimensional seismic modeling experiments. The intent of these experiments is to measure differences in signals between single and multiple sources and between near surface and deeply-buried sources. Theoretical explosion calculations will be compared to the experimental results.

● January 1977, "Seismic Studies for Improved Yield Determination," T. C. Bache, J. M. Savino, M. Baker and P. L. Coleman, SSS-R-77-3108.

The report summarizes the results of the first three months of research on a contract whose main objective is to examine the parameters that affect the seismic signals from underground explosions. Results are presented from research in five areas: 1. theoretical teleseismic magnitudes (M_s and m_b) were determined for a series of nuclear explosion cratering calculations carried out by Applied Theory, Inc.; 2. the relative frequency content of signals from U.S.S.R. and U.S. explosions were studied by comparing the periods of the first few cycles of recordings from several stations at teleseismic ranges; 3. some improved techniques were developed for computing the equivalent point source representation for explosions in highly porous materials; 4. the dependence of body

wave magnitude on yield for underground explosions in salt was studied and compared to that for explosions in granite; 5. small scale experiments were carried out in which underground explosions were modeled by 0.25 gram charges embedded in concrete.

● April 1977, "Seismic Studies for Improved Yield Determination," T. G. Barker, M. Baker, P. Coleman, D. G. Lambert, SSS-R-77-3191.

The report summarizes the results of the second three months of research on a contract whose main objective is to examine the parameters that effect the seismic signals from underground nuclear explosions. Results were presented on research in five areas: 1. data pertinent to regional bias in m_b and M_s in the United States and central Asia were summarized; 2. signals simulating those from multiple explosions were decomposed and scaled by narrow-band filtering methods; 3. numerical simulations of contained explosions were compared with previous laboratory simulations; 4. laboratory experiments of cratering explosions were completed using 0.25 gram charges embedded in concrete; 5. the primary factors controlling amplitude-yield scaling at regional distances were investigated.

● July 1977, "Seismic Studies for Improved Yield Determination," T. C. Bache, P. L. Goupillaud and B. F. Mason, SSS-R-77-3345.

Results are presented from research conducted during the quarter from April to June 1977. Work in three research areas is discussed:

1. The dependence of observed surface wave amplitudes on explosion yield and the characteristics of the emplacement

medium is reviewed. Surface wave data compiled by others is used in conjunction with a new data set consisting of Airy phase amplitudes from the WWSSN stations ALQ and TUC.

2. The theoretical dependence of surface wave amplitude on the important controlling parameters is discussed. Attention is directed to the assumptions of the theoretical models and their consequences.

3. Preliminary results are presented for the development and testing of a deconvolution technique for analyzing short period teleseismic recordings of explosions.

4.2 FINAL CONTRACT REPORTS

- October 1976, " Improved Yield Determination and Event Identification Research," J. M. Savino, T. C. Bache, T. G. Barker, J. T. Cherry, D. G. Lambert, J. F. Masso, N. Rimer and W. O. Wray, SSS-R-77-3038.

Work performed on Contract No. F8606-75-C-0045 has been reported in detail in a series of twelve topical and quarterly technical reports. This final report summarizes the material covered in each of the technical reports and discusses the conclusions obtained. The primary objective of the program is to develop methods for estimating the yield of underground nuclear explosions. The topics addressed include the modeling of both single and multiple explosions, propagation of the resultant stress waves through realistic earth structures, and prediction of short- and long-period explosion seismograms recorded at teleseismically located receivers. The results of these investigations provide a theoretical framework for expressing uncertainties in explosion yield estimates in terms of uncertainties in the near source material properties, local source and receiver crustal structures, and the upper mantle structure of the earth.

● July 1977, "Seismic Ground Motion From Free-Field and Underburied Explosive Sources," M. Baker, J. T. Cherry, and P. L. Coleman, SSS-R-77-3349.

Laboratory experiments were conducted in order to obtain ground motion measurements of free-field and underburied explosive sources. A large negative pulse was observed on the seismograms from the underburied sources. Numerical models indicate that this event is caused by the interaction of the free surface reflection with the containment membrane.

4.3 TECHNICAL REPORTS

● September 1975, "Seismic Coupling From a Nuclear Explosion: The Dependence of the Reduced Displacement Potential on the Nonlinear Behavior of the Near Source Rock Environment," J. T. Cherry, N. Rimer and W. O. Wray, SSS-R-76-2742.

The objective of the research presented in this report is to determine the dependence of teleseismic magnitudes on the nonlinear behavior of the near source rock environment. Such information enables one to express uncertainties in explosive yield estimates in terms of uncertainties in the material properties and provides insight concerning the requirements for collection of geophysical data at a specific test site.

A series of spherically symmetric calculations have been performed in which the properties of the near source material were varied systematically. Output from these calculations enables one to determine the relative teleseismic coupling efficiency of a given near source material. Also, since seismic magnitudes are directly related to explosive yield, this parameter study permits an assessment of uncertainties in the estimated yield in terms of uncertainties of the material properties of the test site.

● October 1975, "Constitutive Equations for Fluid-Saturated Porous Media," S. K. Garg, SSS-R-76-2766.

This report develops constitutive relations for fluid-saturated porous media, suitable for inclusion in standard hydrodynamic codes (e.g., CRAM or SKIPPER). The theoretical formulation is based on the models for fluid-saturated rock aggregates previously developed by Garg and Nur (1973) and Garg, et al., (1975).

● February 6, 1976, "Prediction and Matching of Teleseismic Ground Motion (Body and Surface Waves) From the NTS MAST Explosion," T. G. Barker, T. C. Bache, J. T. Cherry, N. Rimer and J. M. Savino, SSS-R-76-2727.

This report presents the results of a theoretical prediction of the teleseismic body and surface wave signatures of the recent underground explosion, MAST, and a detailed comparison of the predicted waveforms with seismograms recorded at stations of the Special Data Collection System (SDCS). This study represents a comprehensive analysis of the MAST event involving computer modeling of the close-in nonlinear ground motion produced by the explosion, propagation of the resultant stress waves through the appropriate earth structures and computation of seismograms recorded at designated teleseismic stations.

● February 10, 1976, "Teleseismic Coupling From the Simultaneous Detonation of an Array of Nuclear Explosions," J. T. Cherry, T. C. Bache, W. O. Wray and J. F. Masso, SSS-R-76-2865.

This report presents the results of a theoretical stud undertaken to determine if teleseismic ground motion may be enhanced by the simultaneous detonation of a closely spaced array of nuclear explosions. The specific array analyzed con sisted of three 15 kt explosions equally spaced 165 meters apart. The explosive array was assumed contained, i.e., coupling effects due to cratering were not included in the analysis.

- May 1976, "Comparison of Theoretical and Observed Body and Surface Waves for KASSERI, an Explosion at NTS," T. C. Bache, T. G. Barker, N. Rimer and J. M. Savino, SSS-R-76-2937

This report presents the results of a theoretical cal- culation of the teleseismic body and surface waves for the NT KASSERI explosion, and a detailed comparison of the synthetic seismograms with those recorded at stations of the Special Da Collection System (SDCS). This study is a comprehensive anal sis of the KASSERI event including modeling of the close-in nonlinear ground motion produced by the explosion, propagatio of the resulting seismic waves through the earth and computat of synthetic seismograms at designated teleseismic stations.

- May 1976, "Teleseismic Verification of Data Exchange Yields," T. C. Bache, T. G. Barker, J. T. Cherry and J. M. Savino, SSS-R-76-2941.

This working paper addresses the possibility of direct inverting teleseismic ground motion in order to obtain explo- sion yield. We accomplished this inversion via a determinist model which predicts the teleseismic ground motion for a nuclear explosion. Our intent is to use the data to choose a analog rock whose material properties are consistent with the data furnished in the exchange.

● November 1976, "The Dependence of Body Wave Magnitude on Yield for Underground Explosions in Salt," T. C. Bache, J. T. Cherry and B. F. Mason, SSS-R-77-3057.

In this report we address the dependence of body wave magnitude (m_b) on yield for explosions in salt. Our objective is to compare salt events in Eurasia to similar, though hypothetical, events at NTS and to granite events at NTS. Our study uses deterministic computational methods and our results are based on time domain measurements from synthetic seismograms. The methods have been shown to give theoretical seismograms that agree quite well with observations when the appropriate model parameters are included in the calculations.

● January 1977, "Theoretical Body and Surface Wave Magnitudes for Twelve Numerically Simulated Cratering Explosions," T. C. Bache, J. F. Masso and B. F. Mason, SSS-R-77-3119.

The results of the Systems, Science and Software (S^3) contribution to a study of cratering explosions are presented. A series of twelve numerical simulations of 150 kt cratering explosions in three materials at several depths were carried out by Applied Theory, Incorporated. The data from these calculations were processed to compute theoretical far-field body and surface wave seismograms and from these to determine m_b and M_s. The m_b and M_s data is to be analyzed by Pacific Sierra Research.

The theoretical seismogram calculations are done in a two-step process. First, an equivalent elastic source representation of the cratering event is obtained. The wave field is then propagated through realistic layered earth models to teleseismic distances. For this application the procedure is found to be more accurate for the shorter period body waves

than for the surface waves. The m_b and M_s values are presented for the twelve 150 kt sources and for these sources scaled to 37.5 and 600 kt. Also given are the values for contained explosions of the same yield in the same emplacement material. The contribution of the ejecta fallback is studied and is found to be insignificant for teleseismic magnitude values.

- February 1977, "Comparison of Theoretical and Observed Short Period Seismograms for Soviet Explosions in Salt," T. C. Bache, SSS-CR-77-3136. (Classified Report, Unclassified Title and Abstract.)

In this report we direct our attention to five specific Soviet explosions in salt. These were PNE events and the Soviet estimates for the yield and depth of burial are available. The contracting officer has also provided us with estimates of the near-source crustal layering for these events. The question to be addressed in our report is then, with all this information, how well can we match the recorded waveforms and amplitudes for these events? (U)

- March 1977, "A Review of the Nature and Variability of the Anelastic Properties of the Upper Mantle Beneath North America and Eurasia," B. J. Mitchell and T. C. Bache, SSS-R-77-3164.

All reasonable mechanisms for producing low-velocity zones in the upper mantle should also produce zones of low Q. The available studies of upper mantle Q and velocity for the same regions suggest that a coincidence of low velocity and low Q zones does indeed occur.

Seismic body- and surface-wave data indicate a substantial low velocity, low Q zone in the upper mantle beneath western North America. The zone appears to be 150 km thick

or more, the velocities for both P and S waves being lower than typical upper mantle velocities for stable regions.

The available evidence for eastern North America indicates that a low velocity zone is either absent for that region or more poorly developed than it is in western North America. Most interpretations for P waves in eastern North America include no low velocity zone. Surface wave studies of the shear wave velocity structure beneath eastern North America indicate the possibility of a low velocity zone for S waves, at least in some regions.

The available data for northern Europe and Asia indicate that it is a stable region with velocity and attenuative properties much like those of eastern North America. The difference in attenuative properties of the upper mantle between the western United States and northern Asia might lead to higher m_b values for the Asian nuclear events than for equivalent NTS events, if the low velocity, low Q zone beneath the western United States is sufficiently thick and has low enough values. Thickness and Q values suggested by most published research can easily cause m_b values for events in the Basin and Range province to be a few tenths of a magnitude unit lower than events in shield regions.

● June 1977, "Simulation and Decomposition of Multiple Explosions," D. G. Lambert, T. C. Bache and J. M. Savino, SSS-R-77-3194.

The purpose of the study is to develop procedures for using seismic measurements to verify the number and yields of individual explosions making up a multiple event. Multiple explosion seismograms are simulated by straightforward summations of single explosion records. Several types of multiple explosions are simulated. These include closely spaced equal yield explosions (no consideration given to propagation path

effects between explosions and receiver) and relatively more widely spaced explosions (propagation path effects included) of varying yields. The data employed are principally close-in seismic recordings of the Nevada Test Site explosions obtained from Sandia Laboratories in Albuquerque, New Mexico. Decomposition of the simulated multiple explosion records is accomplished using a series of narrow-band filters with center frequencies ranging from 3 to 100 Hz. In general, our results show that the narrow-band filter technique is able to achieve accurate time separation and amplitude scaling. The limitation on the technique is essentially the requirement for the presence of sufficient signal energy at frequencies greater than about 3.5 times the inverse of the lag time between arriving signals.

- October 1977, "Identification of Individual Events in a Multiple Explosion from Teleseismic Short Period Body Wave Recordings," D. G. Lambert and T. C. Bache, SSS-R-78-3421.

The objective of this study is to detect and identify the individual events in a hypothetical multiple explosion. The data analyzed are simulated short period body wave recordings of that event. These were, presumably, constructed by lagging, scaling and summing a single event record according to some formula unknown to the analysts. Data for two stations, including both the single event and multiple event records, were provided to Systems, Science and Software by the VELA Seismological Center (VSC).

The data were analyzed by the MARS (Multiple Arrival Recognition System) program which uses a series of narrow-band filters to identify phase arrivals. Their amplitude and arrival time are accurately preserved. The variable

frequency magnitude (VFM) discriminant is also computed and the multiple explosion records are clearly identified as being from an explosion.

For decomposition of the multiple event the MARS output for the single and multiple event records were cross-correlated. Two main groups of events separated by 6.7 to 7.8 seconds, depending on azimuth, are identified. Each of these groups appears to include two or more explosions. The arrival times and relative yields of the identified events are tabulated for subsequent comparison with the actual values by VSC.